Electronic Supplementary Material (ESI) for New Journal of Chemistry.

Synthesis, self-assembly and Biolabeling of Perylene diimide-Tyrosine Alkyl Amide based Amphiphiles: Nanomolar detection of AOT Surfactant

Poonam Sharma [a], Neha Sharma[b], Satwinderjeet Kaur[b] and Prabhpreet Singh*[a]

[a]*Department of Chemistry, UGC Centre for Advanced Studies II, Guru Nanak Dev University, Amritsar 143 005, India. Tel: +91-84271-01534*

[b]*Department of Botanical and Environmental Sciences, Guru Nanak Dev University, Amritsar 143 005, India.*

Email: prabhpreet.chem@gndu.ac.in

Synthetic Detail:

Synthesis of methyl 6-Aminohexanoate hydrochloride

Dissolve 6-Aminocaproic acid (2 g, 0.015 mol) in 60 ml CH_3OH. Keep round bottom flask at 0°C. Then add $SOCl_2$ (2.77 ml, 0.038 mol) dropwise and continue the reaction on stirring for 10 h at room temperature. After this time interval, the solvent was evaporated and 6-Aminocaproic methyl ester hydrochloride was isolated after triturating the residue with diethyl ether. This triturating procedure was repeated three times to remove the traces of $SOCl_2$ from whitish precipitate of 6-Aminocaproic methyl ester hydrochloride.

^{1}H NMR (400 MHz, DMSO-d_6, 25°C) δ 3.57 (s, -OCH_3, 2H), 2.70 (t, J= 8 Hz, 2H), 2.28 (t, *J* = 7.6 Hz, 2H), 1.59 – 1.43 (m, 4H), 1.32 – 1.25 (m, 2H).

^{13}C NMR (100 MHz, DMSO-d_6, 25°C) δ 173.7, 51.7 (-OCH_3), 38.9, 33.5, 27.0, 25.8, 24.4.

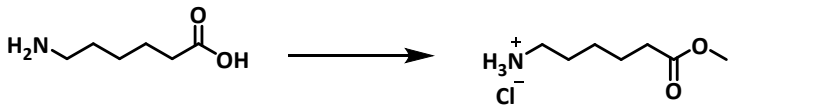

6-aminohexanoic acid — 6-methoxy-6-oxohexan-1-aminium chloride

1. Characterization data of Precursors and target derivatives

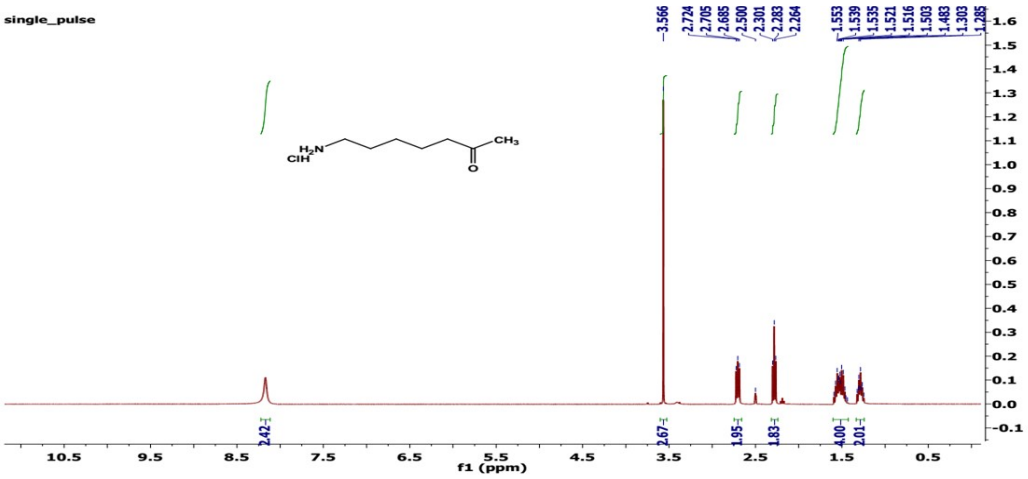

Figure S1a: [1]H NMR spectrum of 6-aminocaproic methyl ester hydrochloride in DMSO-d_6.

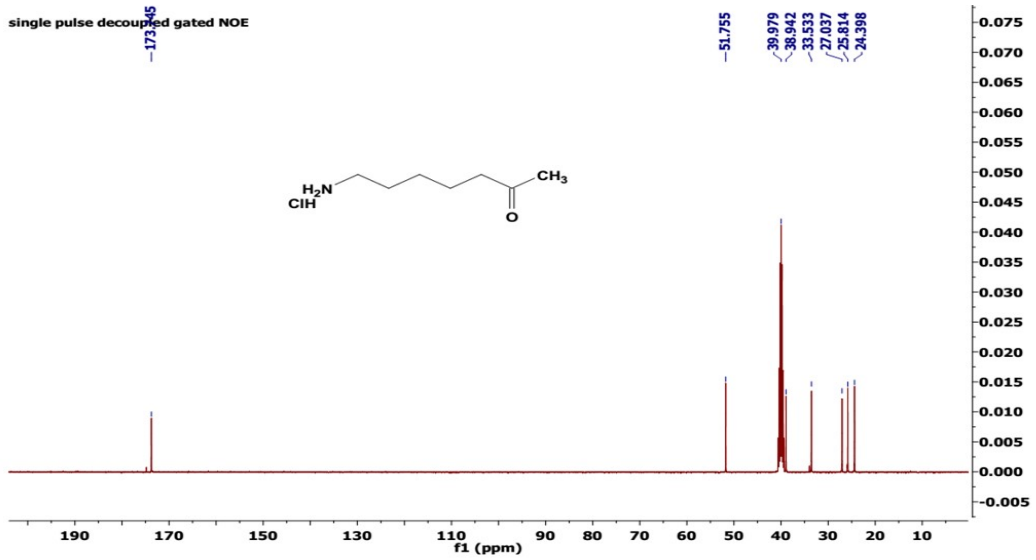

Figure S1b: [13]C NMR spectrum of 6-aminocaproic methyl ester hydrochloride in DMSO-d_6.

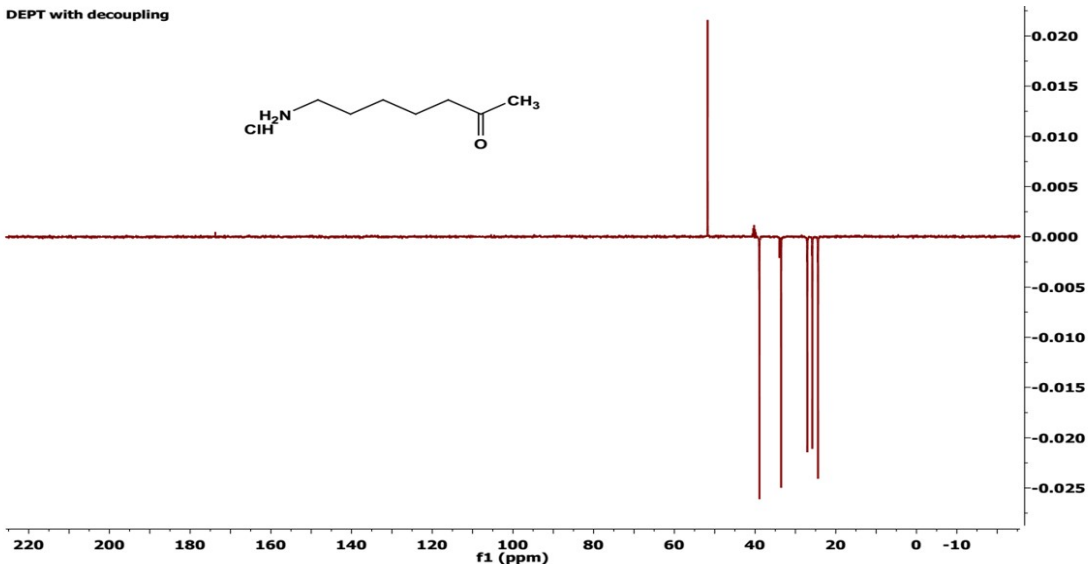

Figure S1c: DEPT-135 spectrum of 6-aminocaproic methyl ester hydrochloride in DMSO-d_6.

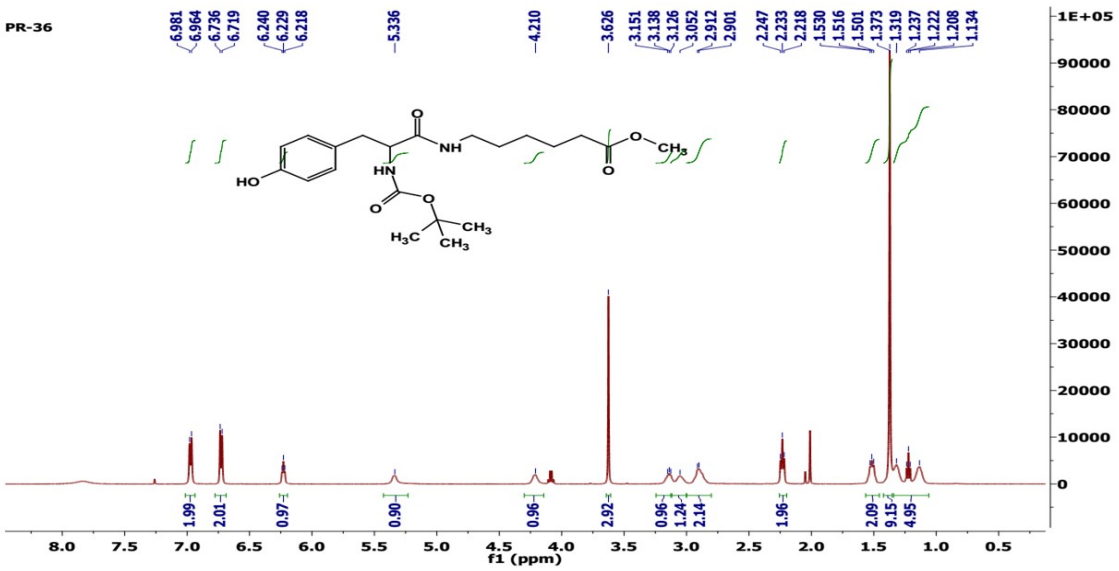

Figure S2a: ^{1}H NMR spectrum of **1c** in $CDCl_3$.

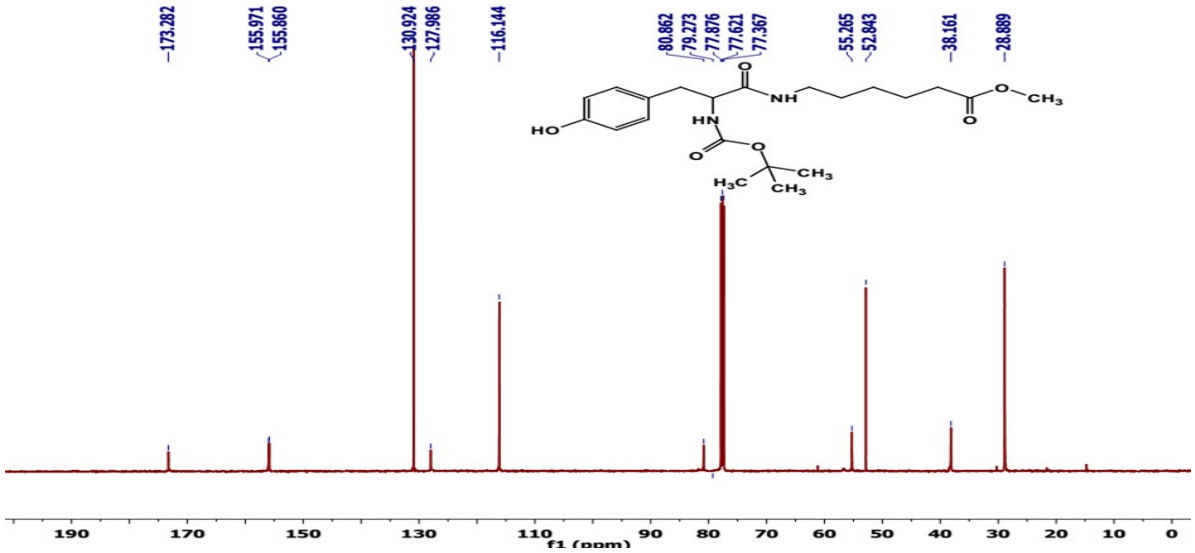

Figure S2b: ^{13}C NMR spectrum of **1c** in $CDCl_3$.

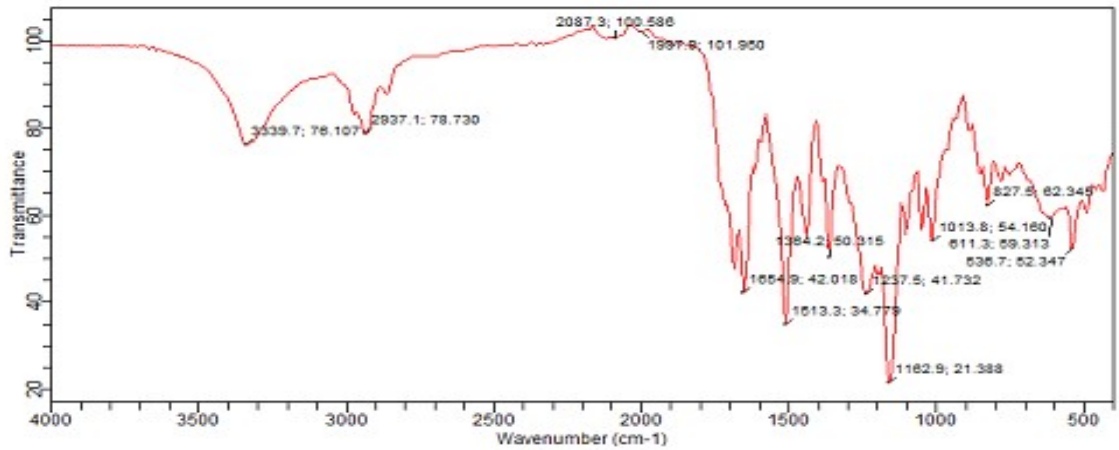

Figure S2c: FTIR spectrum of **1c**.

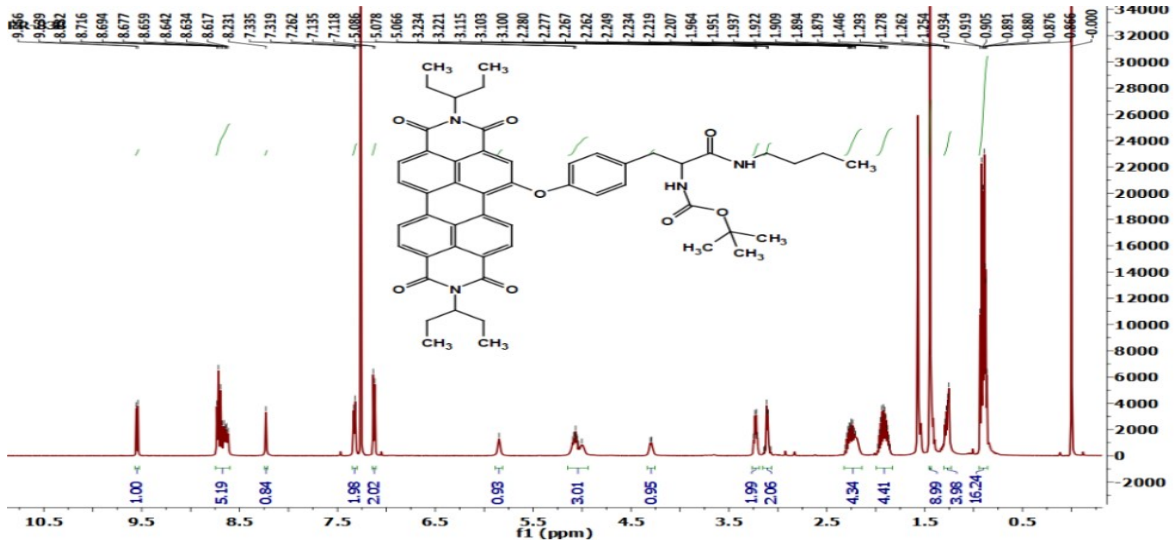

Figure S3a: ^{1}H NMR spectrum of PDI **2a** in $CDCl_3$.

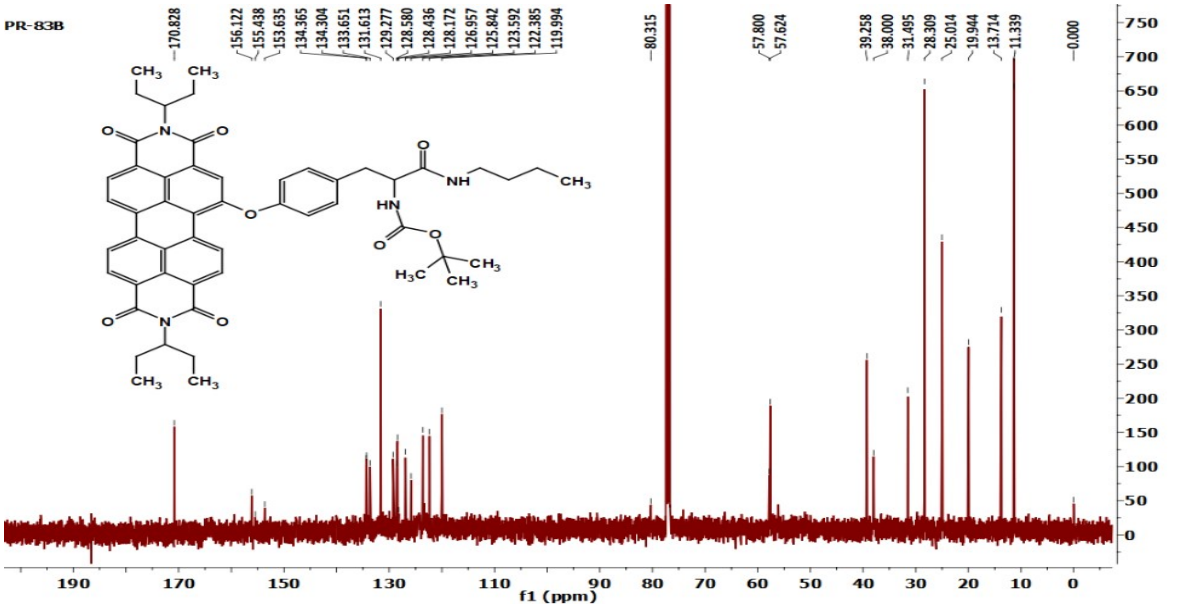

Figure S3b: ^{13}C NMR spectrum of PDI **2a** in $CDCl_3$.

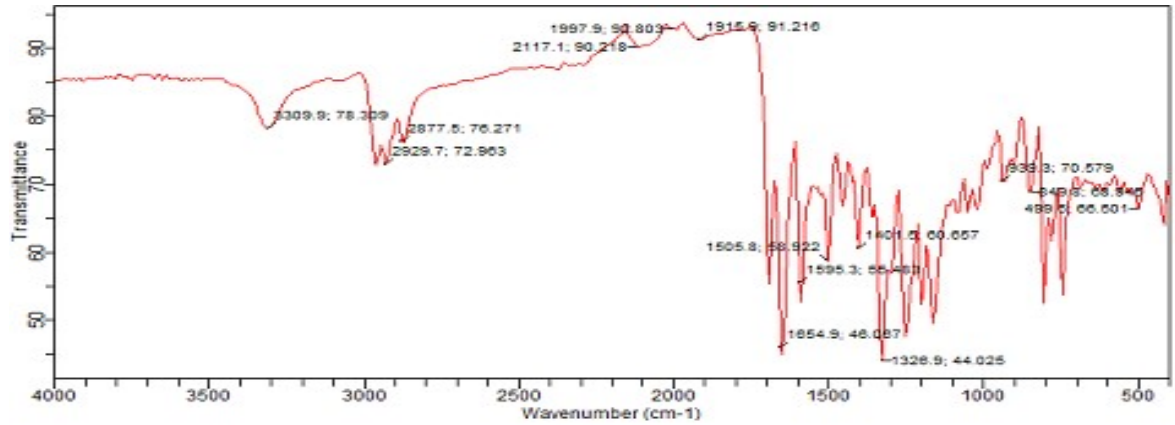

Figure S3c: FTIR spectrum of PDI **2a**.

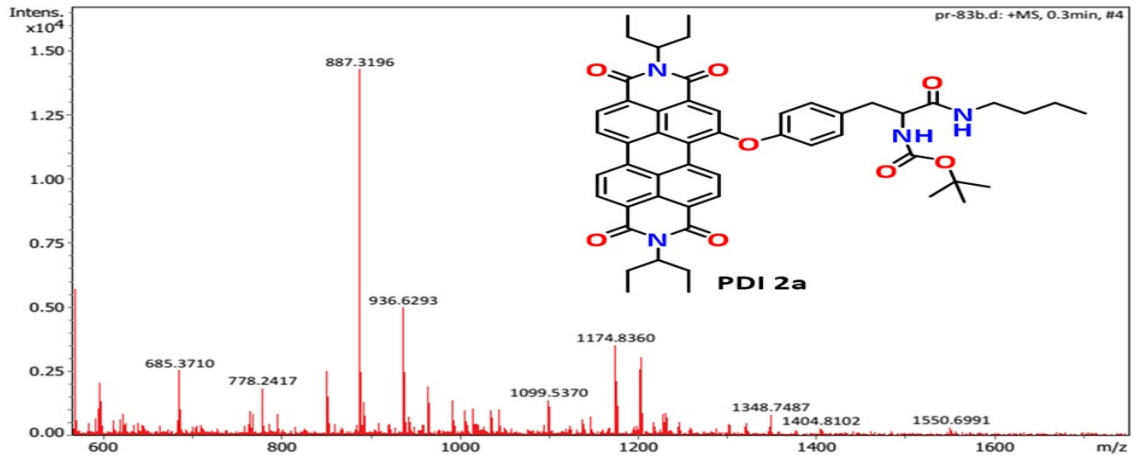

Figure S3d: Mass spectrum of PDI **2a**.

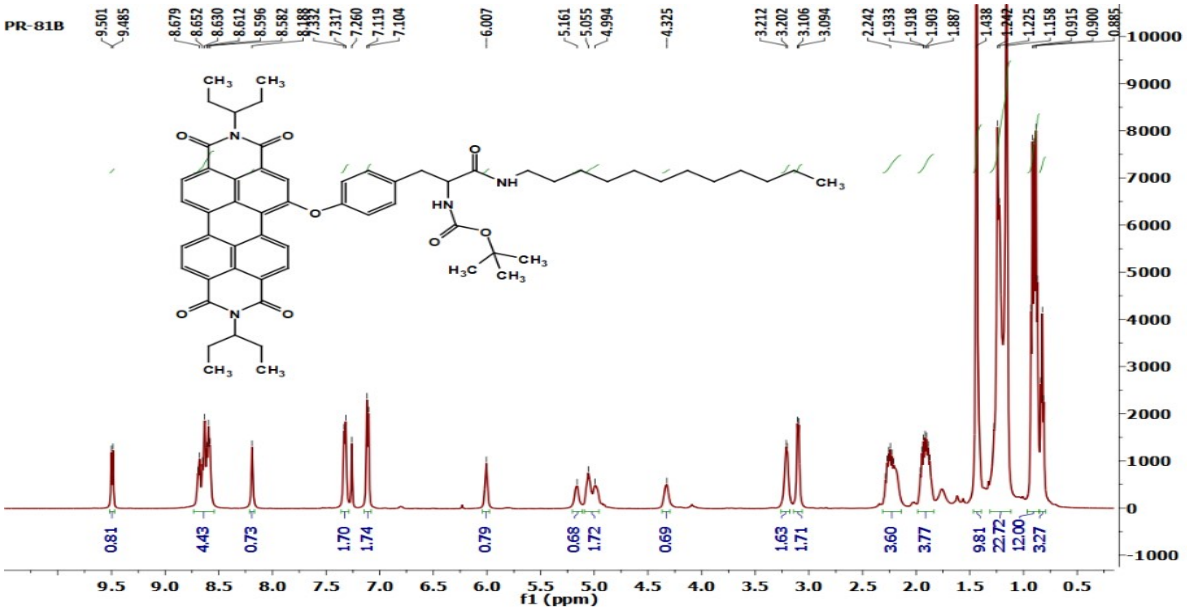

Figure S4a: ^{1}H NMR spectrum of PDI **2b** in $CDCl_3$.

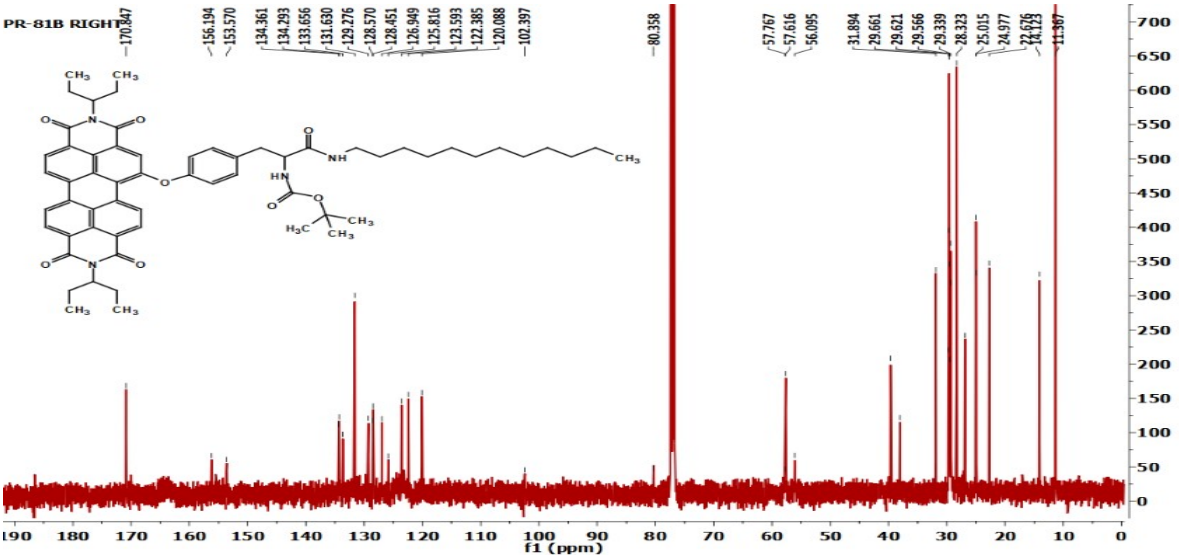

Figure S4b: ^{13}C NMR spectrum of PDI **2b** in $CDCl_3$.

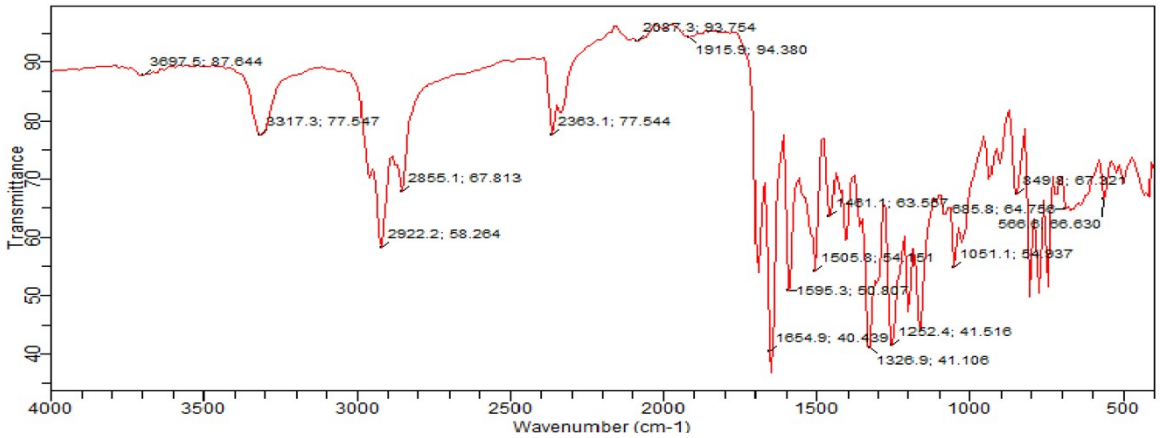

Figure S4c: FTIR spectrum of PDI **2b**.

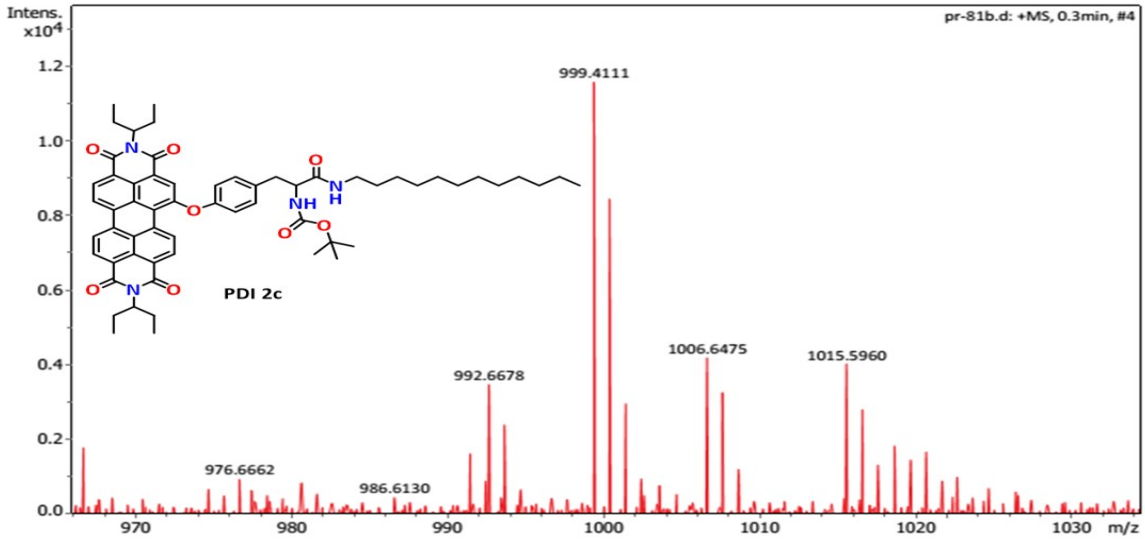

Figure S4d: Mass spectrum of PDI **2b**.

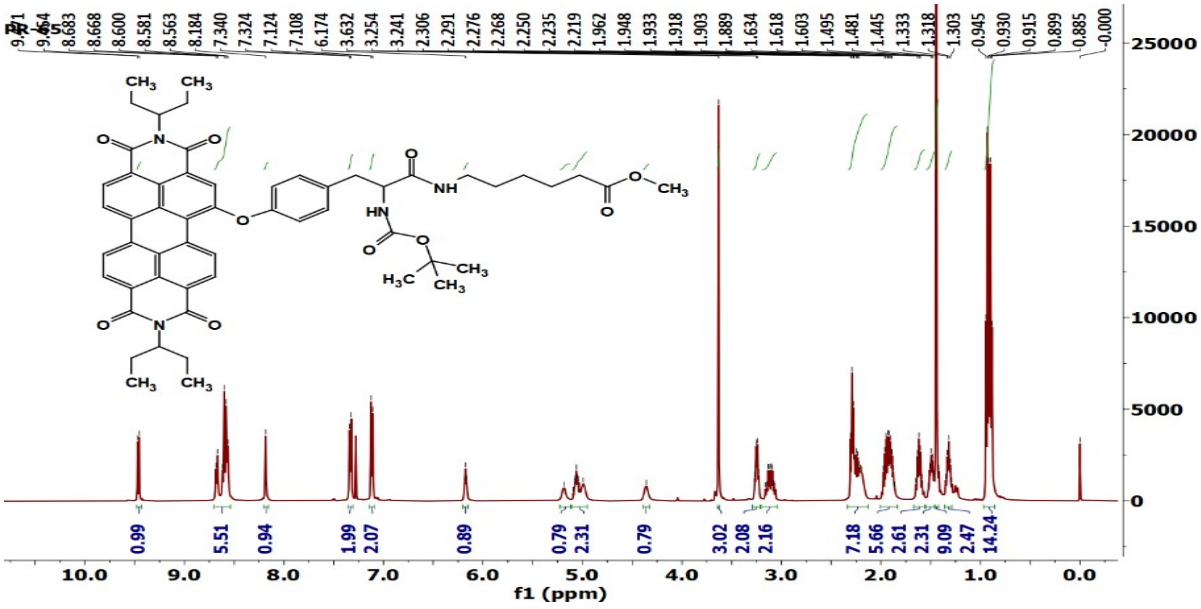

Figure S5a: ^{1}H NMR spectrum of PDI **2c** in $CDCl_3$.

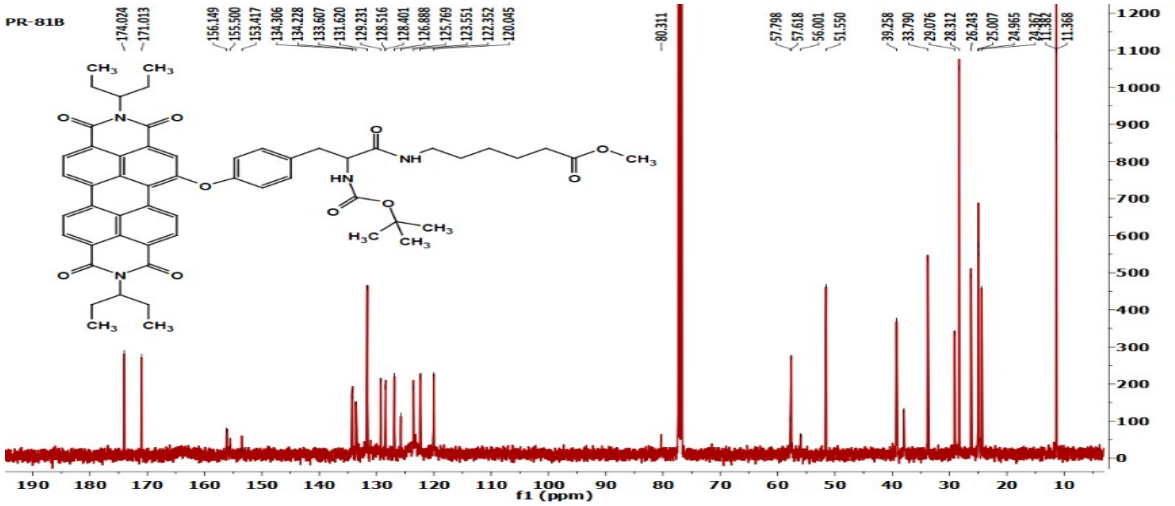

Figure S5b: ^{13}C NMR spectrum of PDI **2c** in $CDCl_3$.

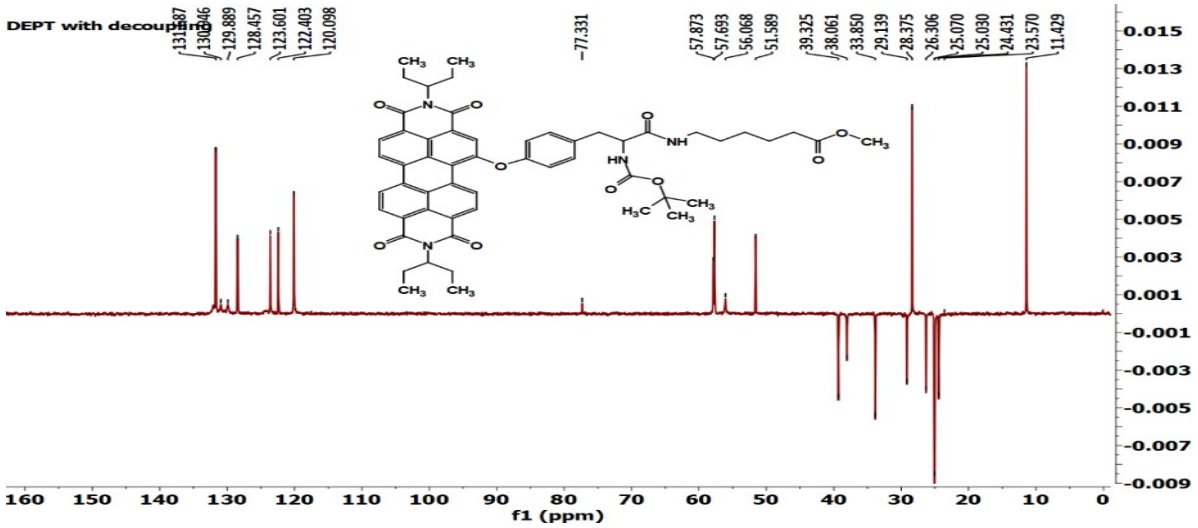

Figure S5c: DEPT-135 spectrum of PDI **2c** in $CDCl_3$.

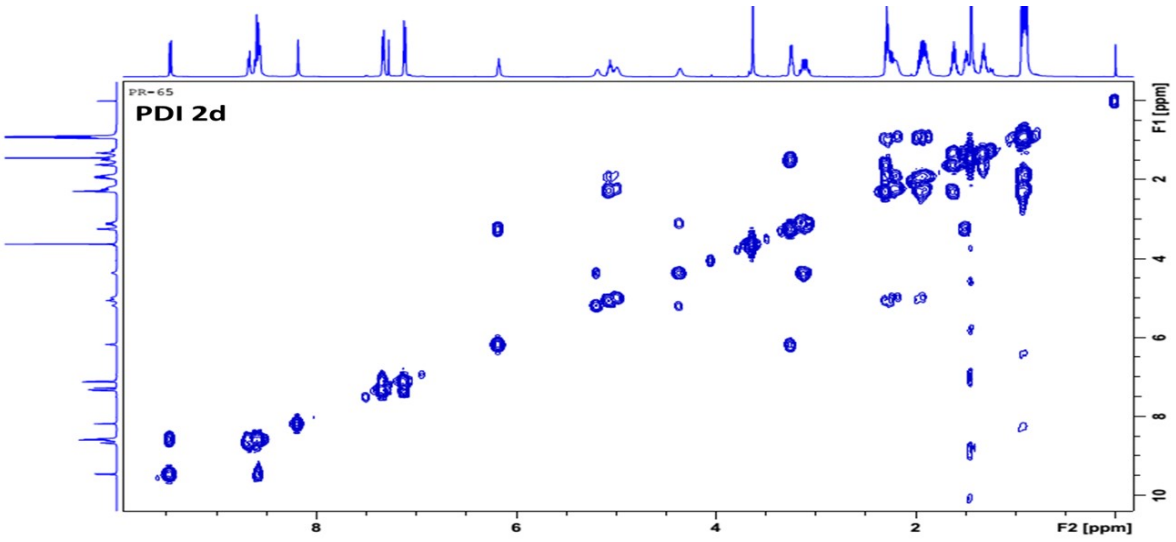

Figure S5d: ^{1}H–^{1}H COSEY NMR spectrum of PDI **2c** in $CDCl_3$.

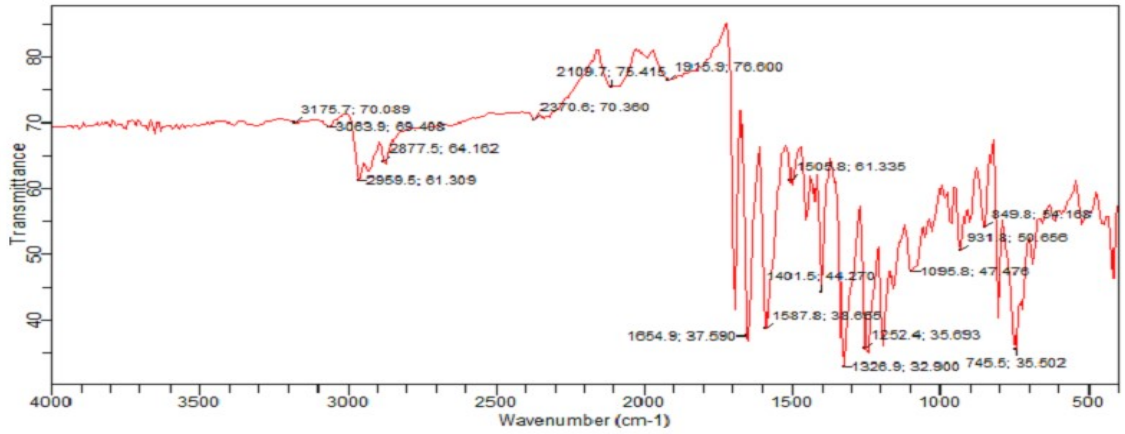

Figure S5e: FTIR spectrum of PDI **2c**.

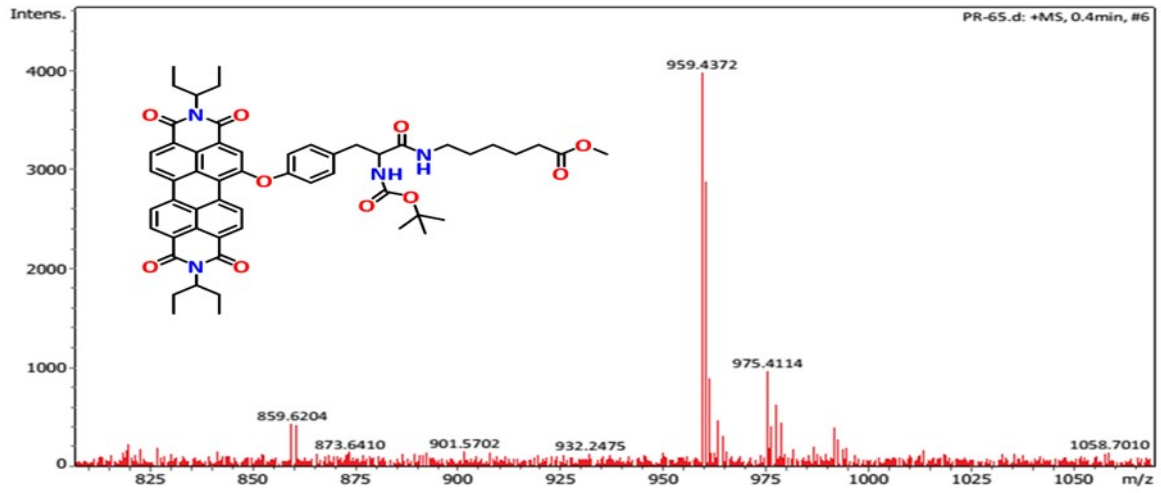

Figure S5f: Mass spectrum of PDI **2c**.

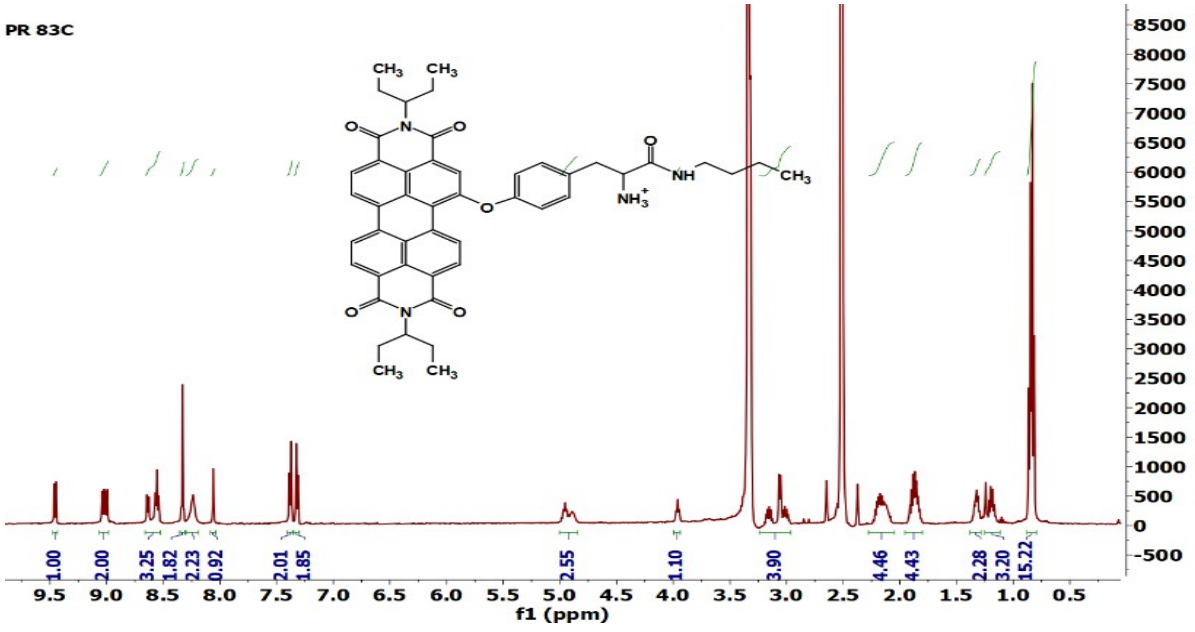

Figure S6a: ^{1}H NMR spectrum of PDI **3a** in $CDCl_3$.

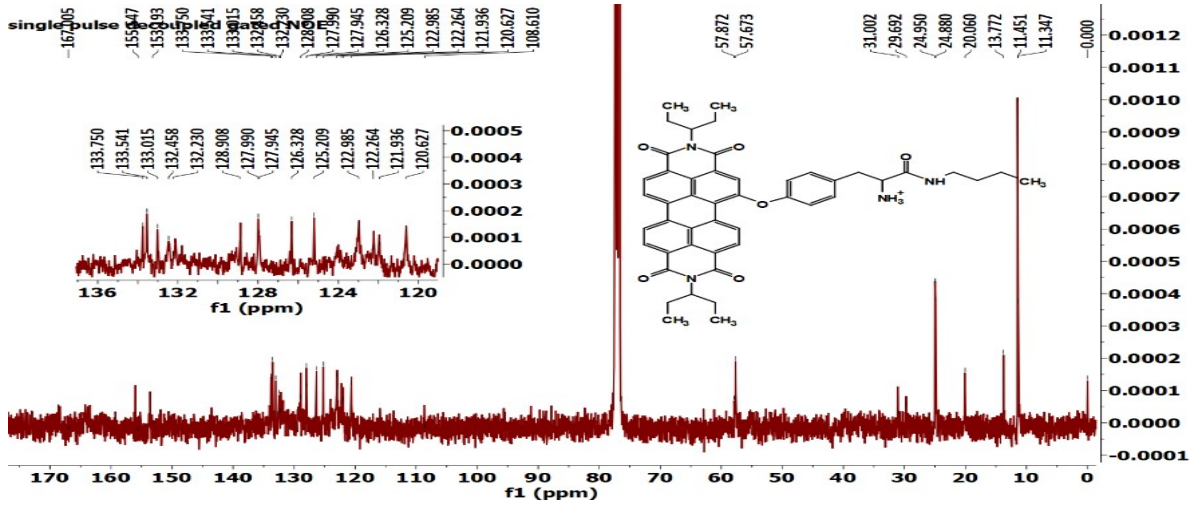

Figure S6b: ^{13}C NMR spectrum of PDI **3a** in $CDCl_3$.

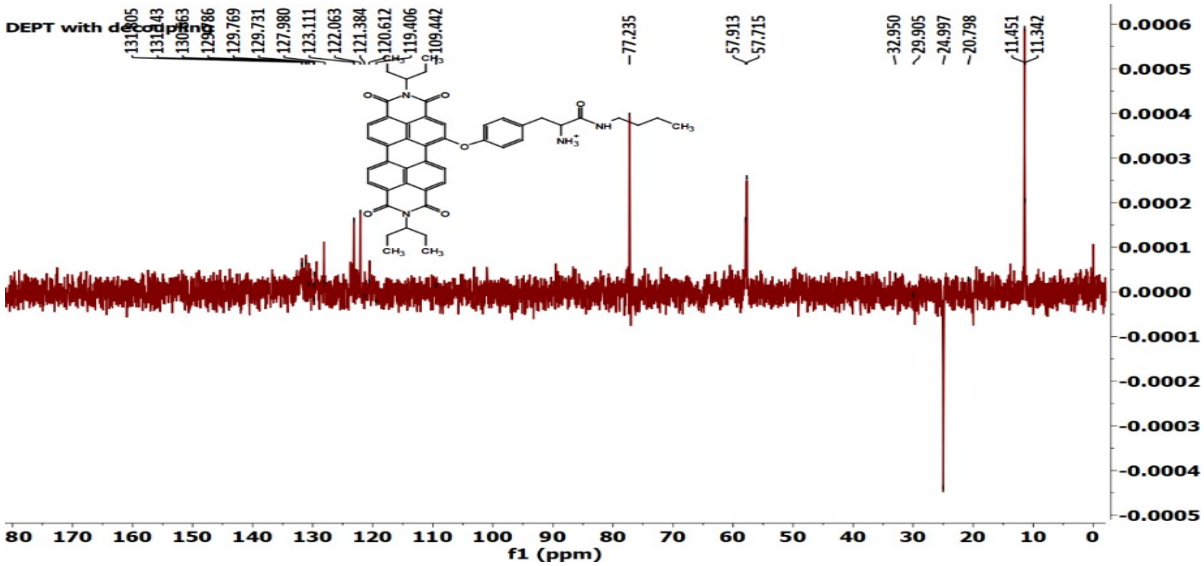

Figure S6c: DEPT-135 spectrum of PDI **3a** in $CDCl_3$.

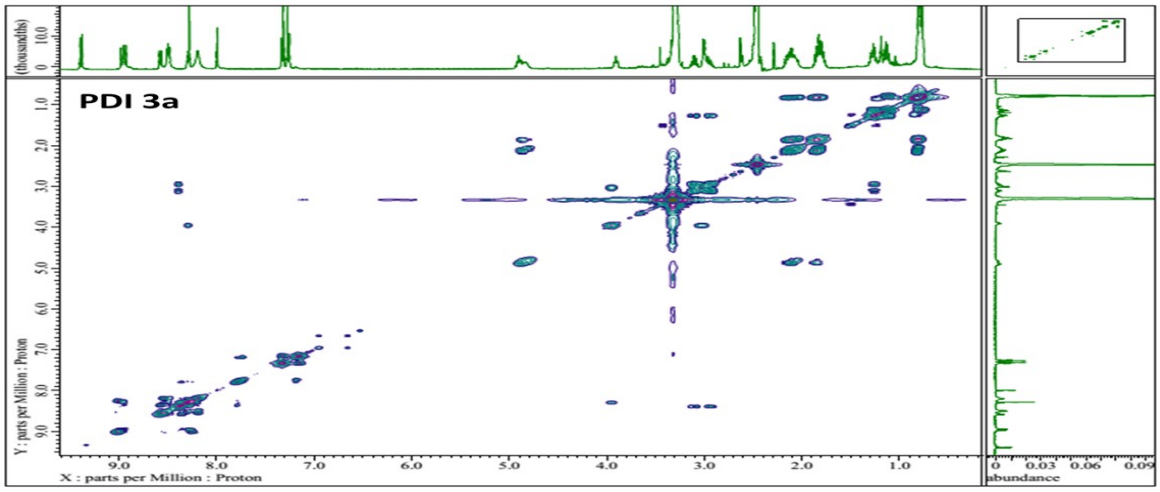

Figure S6d: ^{1}H–^{1}H COSEY NMR spectrum of PDI **3a** in $CDCl_3$.

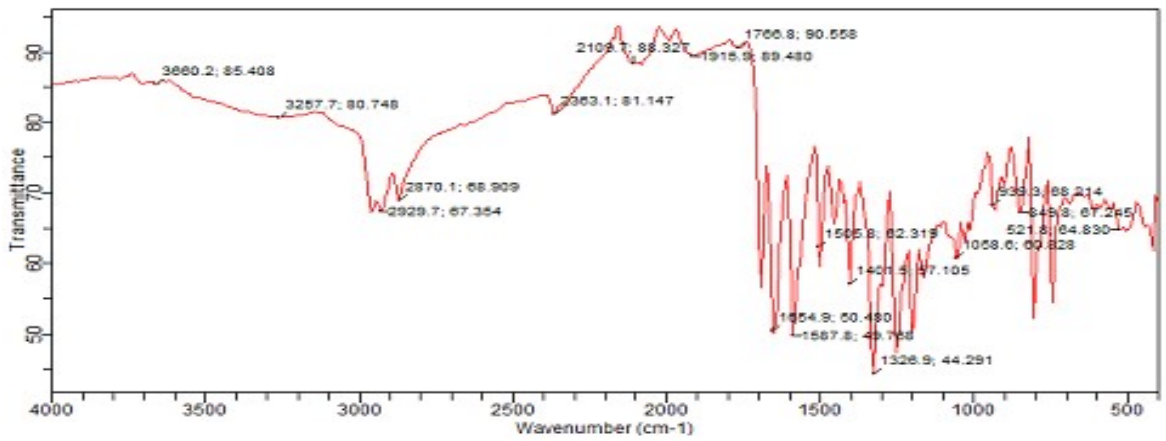

Figure S6e: FTIR spectrum of PDI **3a**.

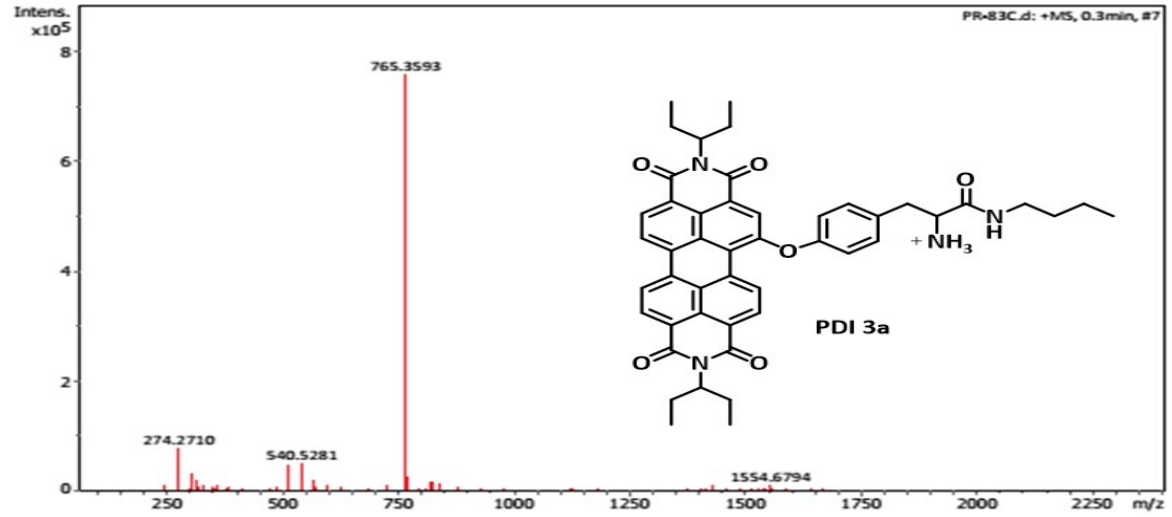

Figure S6f: Mass spectrum of PDI **3a**.

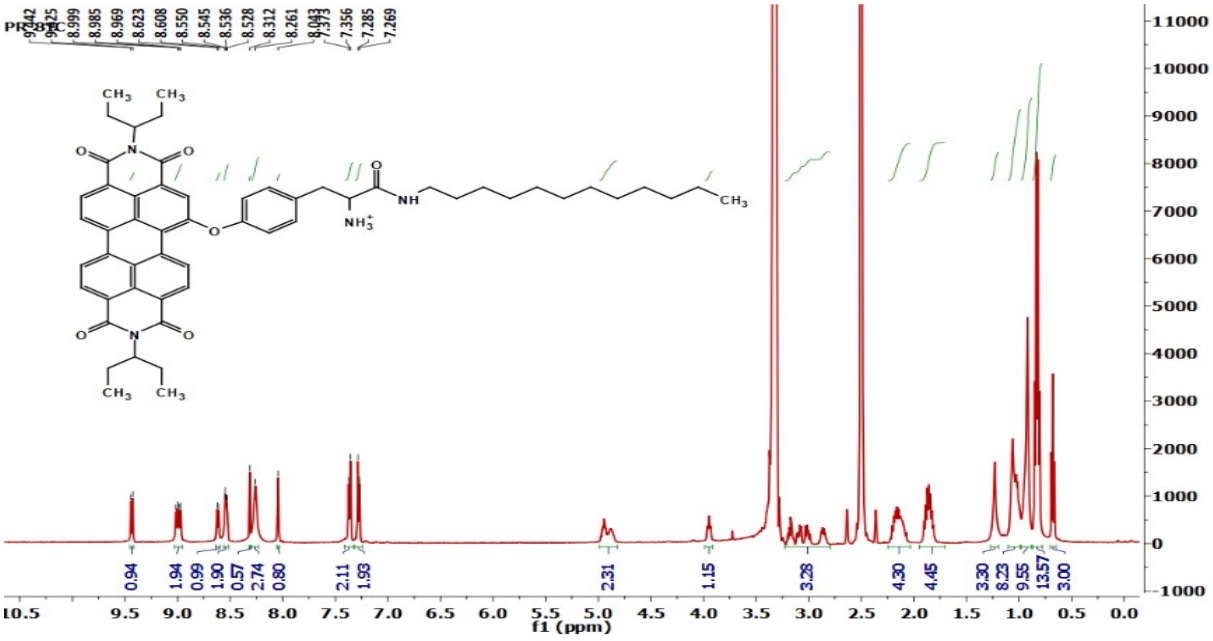

Figure S7a: ^{1}H NMR spectrum of PDI **3b** in $CDCl_3$.

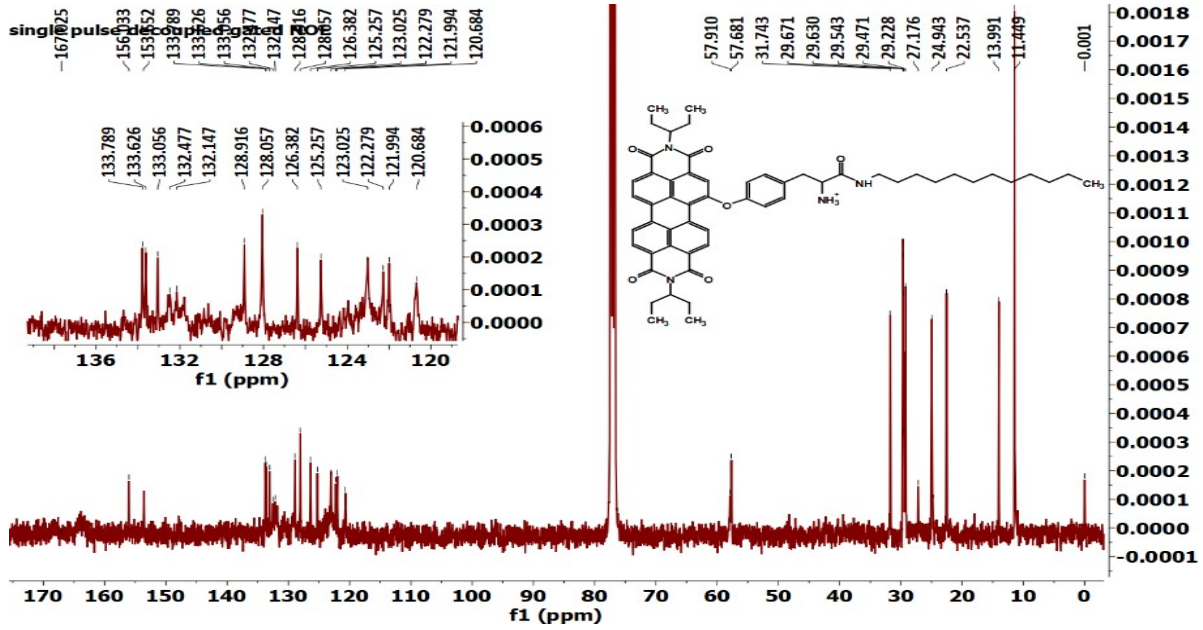

Figure S7b: ^{13}C NMR spectrum of PDI **3b** in $CDCl_3$.

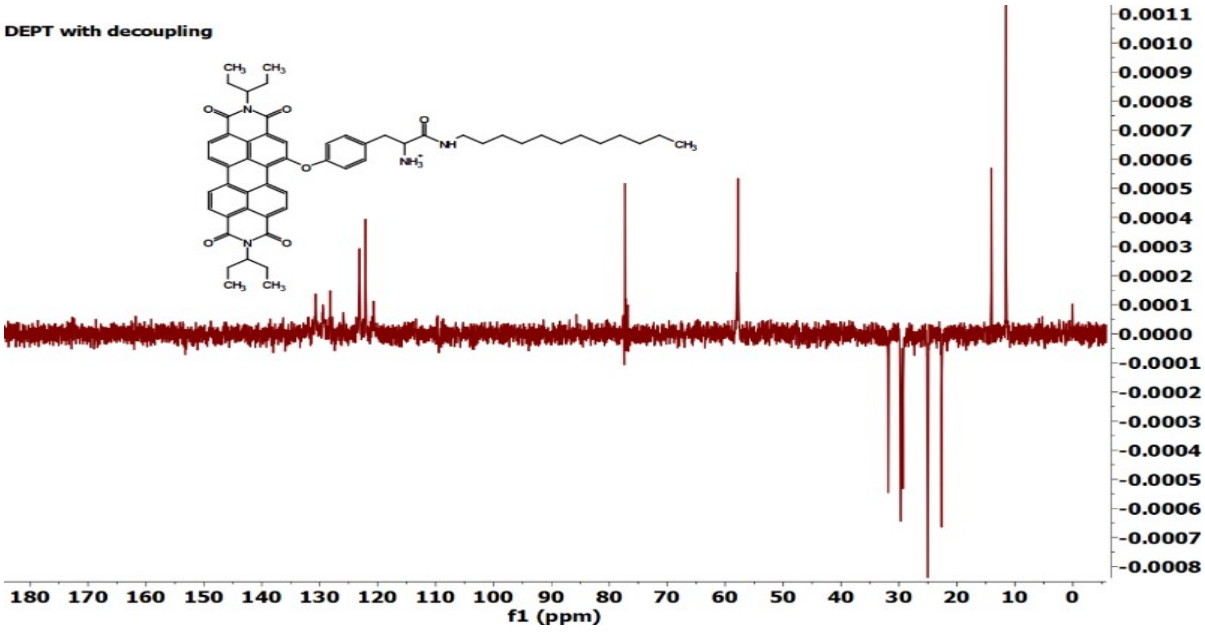

Figure S7c: DEPT-135 spectrum of PDI **3b** in $CDCl_3$.

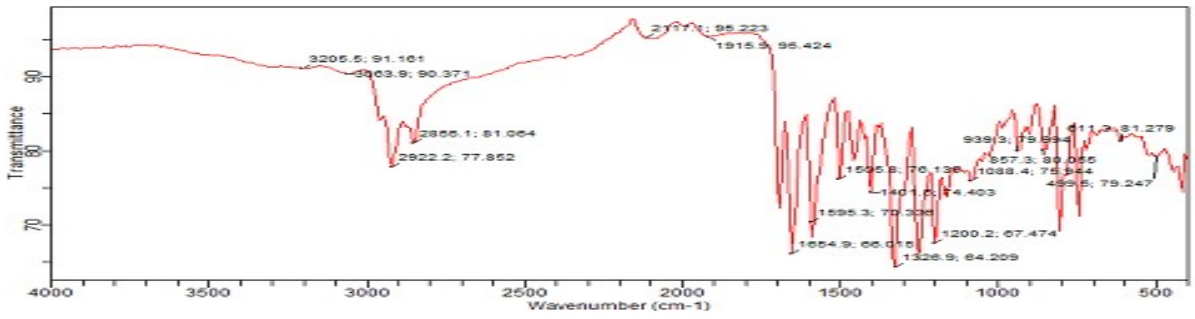

Figure S7d: FTIR spectrum of PDI **3b**.

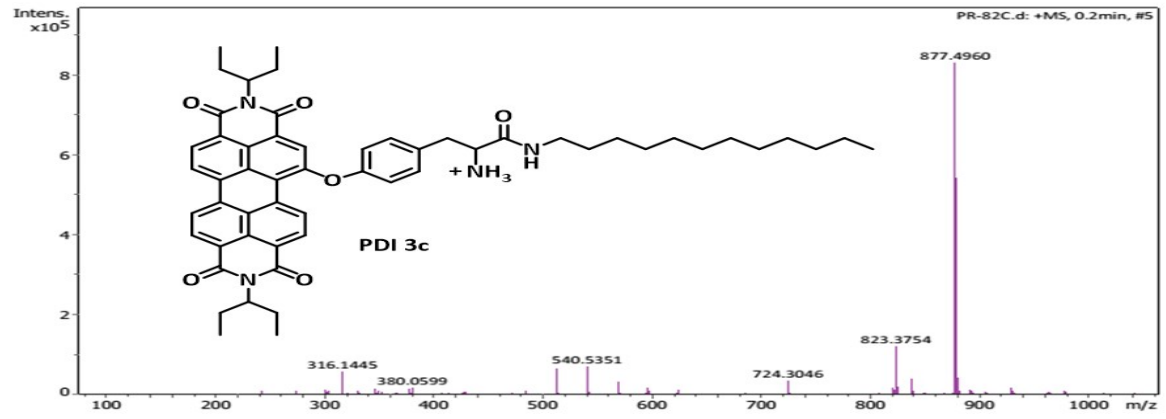

Figure S7e: Mass spectrum of PDI **3b**.

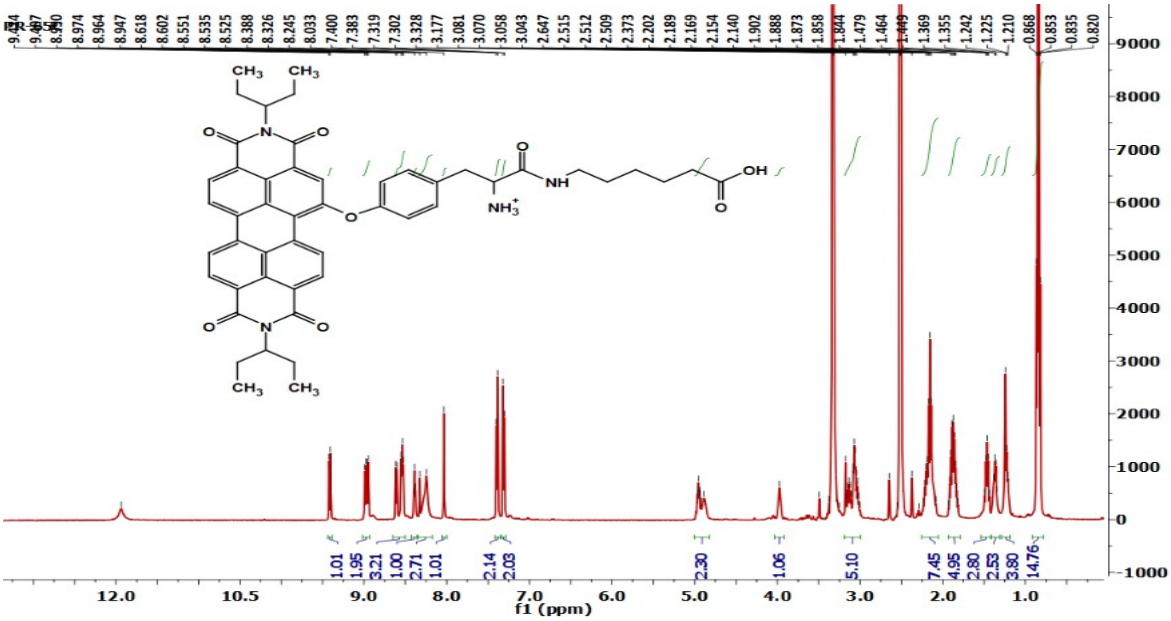

Figure S8a ^{1}H NMR spectrum of PDI **3c** in $CDCl_3$.

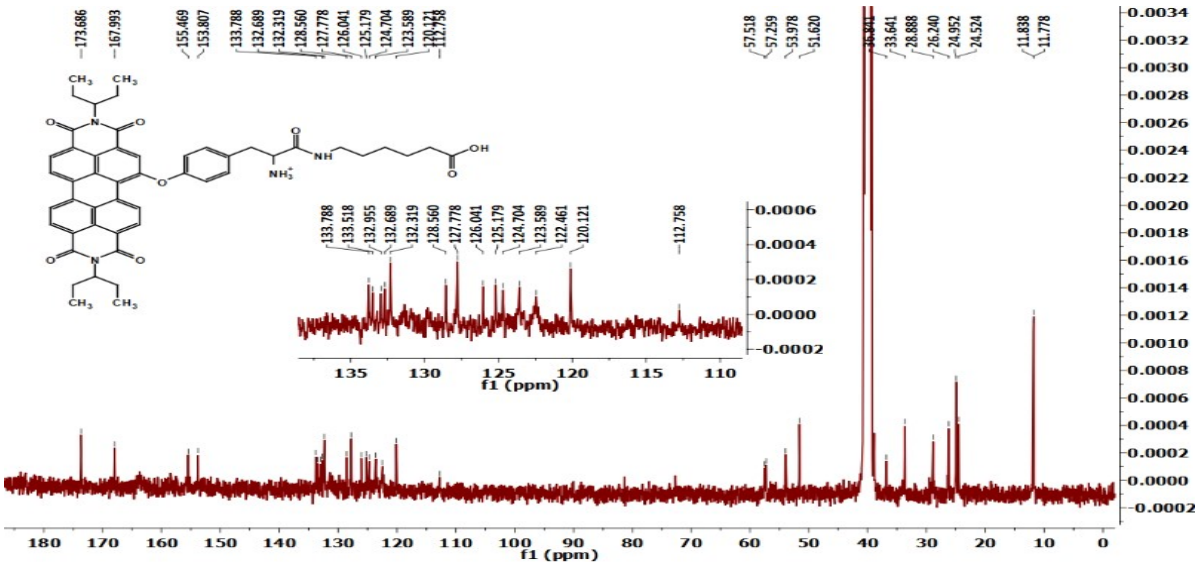

Figure S8b: ^{13}C NMR spectrum of PDI **3c** in $CDCl_3$.

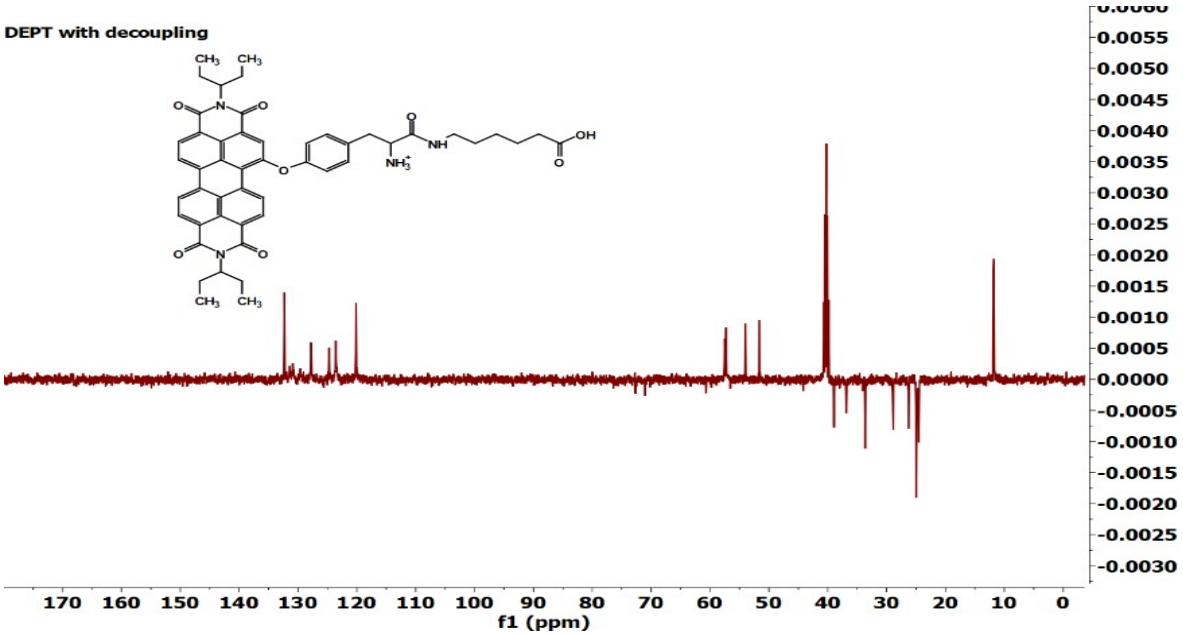

Figure S8c: DEPT-135 spectrum of PDI **3c** in $CDCl_3$.

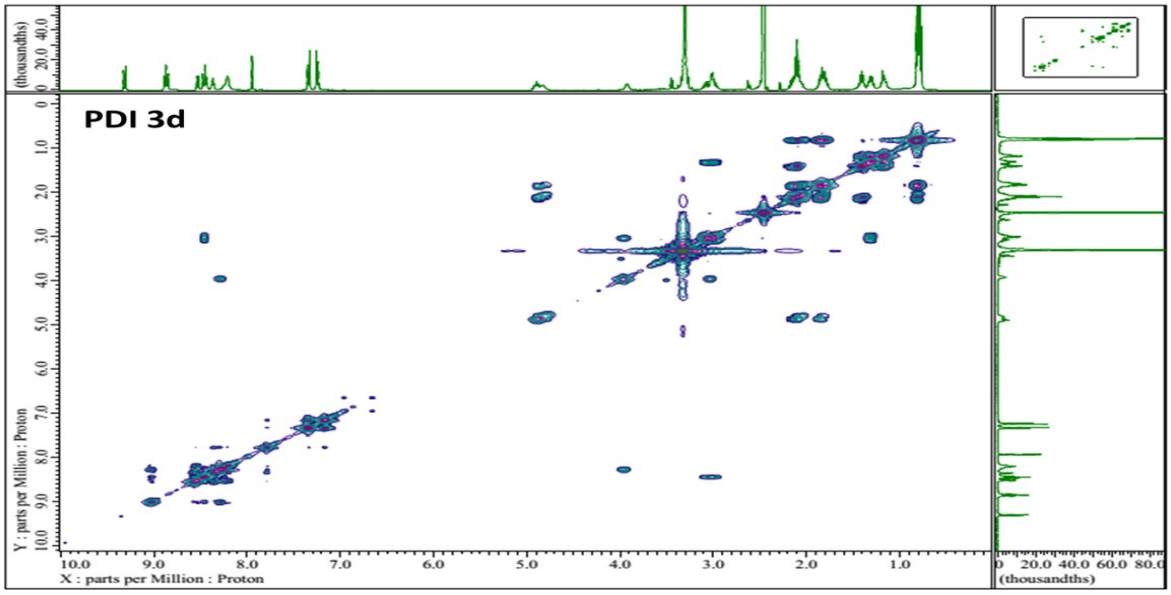

Figure S8d: ^1H–^1H COSEY NMR spectrum of PDI **3c** in $CDCl_3$.

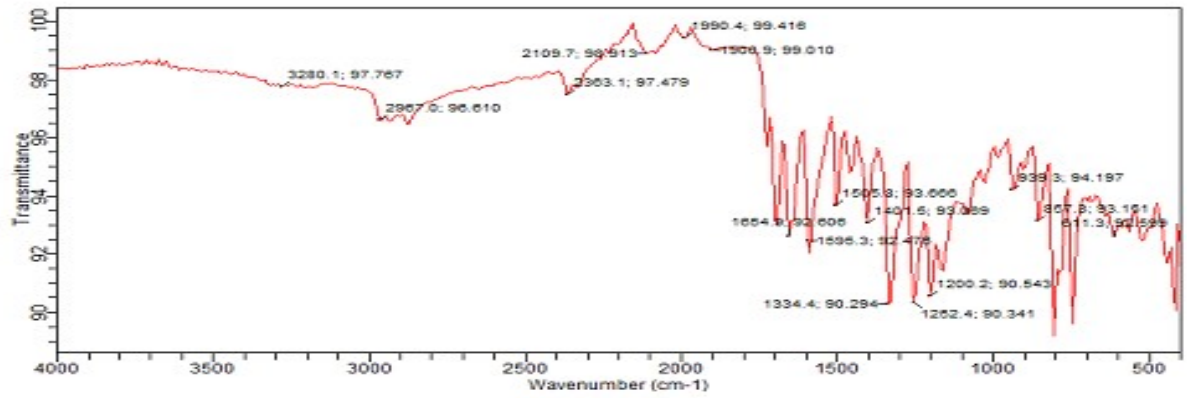

Figure S8e: FTIR spectrum of PDI **3c**.

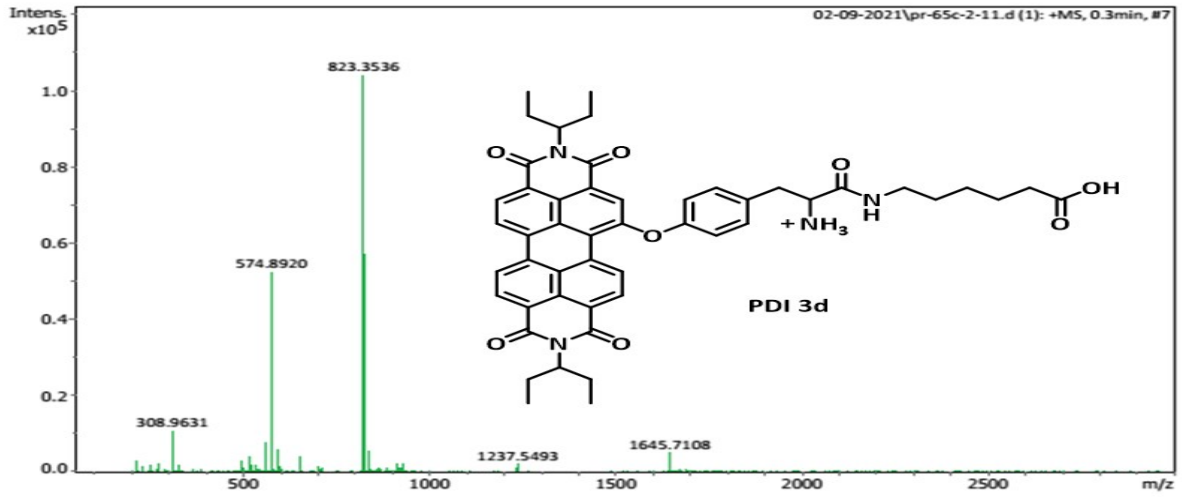

Figure S8f: Mass spectrum of PDI **3c**.

2. Optical data of PDI 2a-2d and PDI 3a-3d

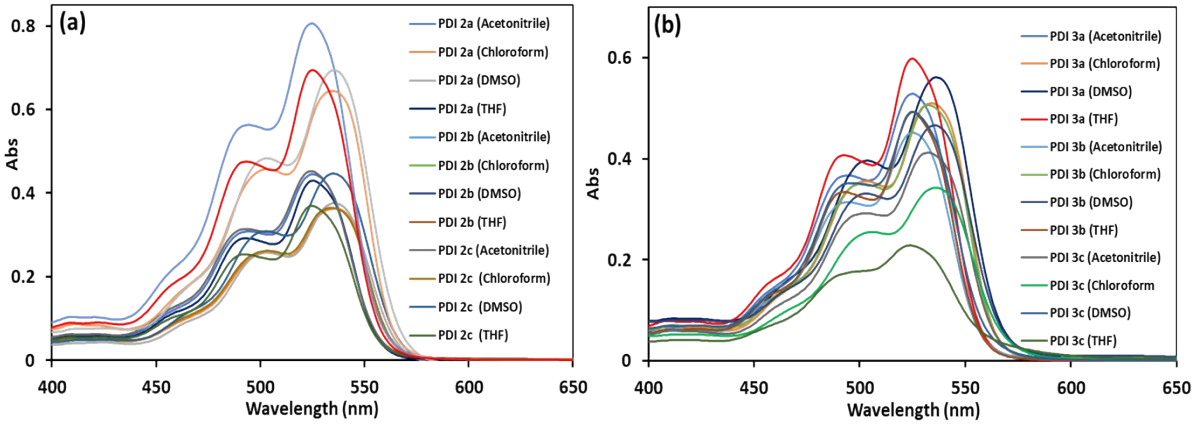

Figure S9: UV–Vis spectra of (a) PDI **2a–2c** (10 µM); (b) PDI **3a–3c** (10 µM) in different polarity solvents.

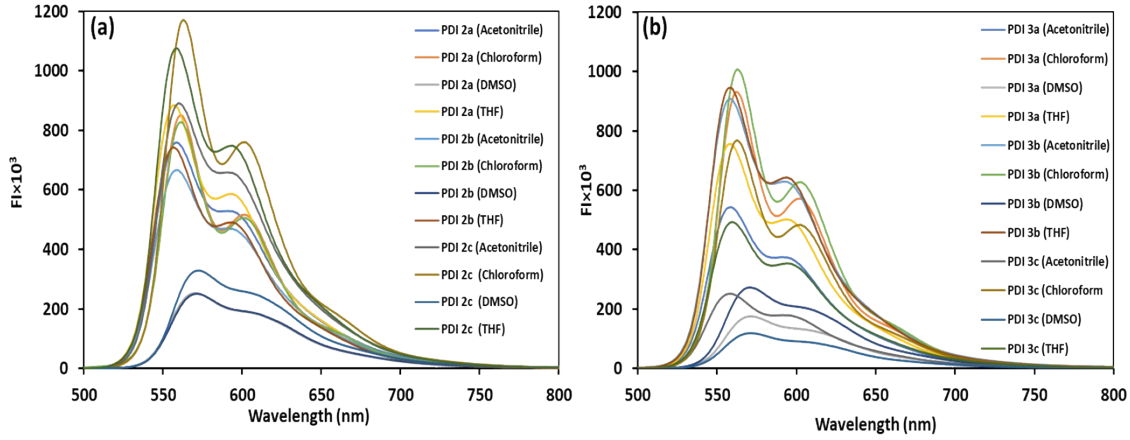

Figure S10: Fluorescence spectra of (a) **PDI 2a–2c** (10 µM); (b) **PDI 3a–3c** (10 µM) recorded in different polarity solvents; λ_{ex} = 490 nm, slit width (ex/em) =5/5.

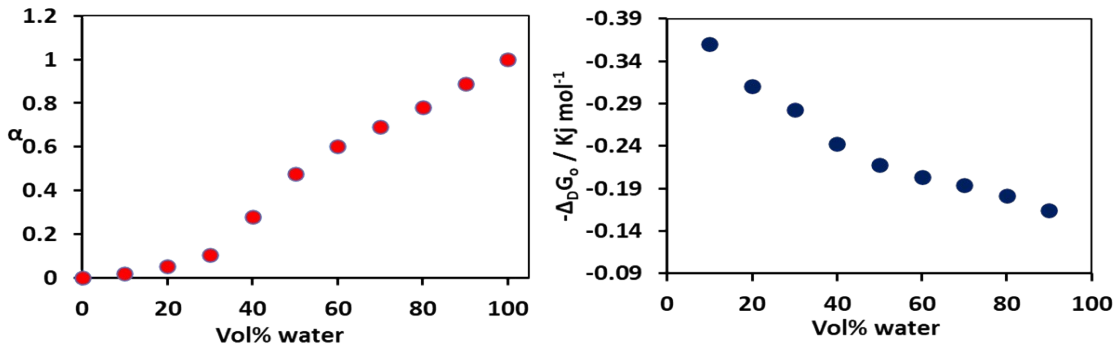

Figure S11a: Plot between degree of aggregation (α) and ΔG and volume % of water for PDI **3a**.

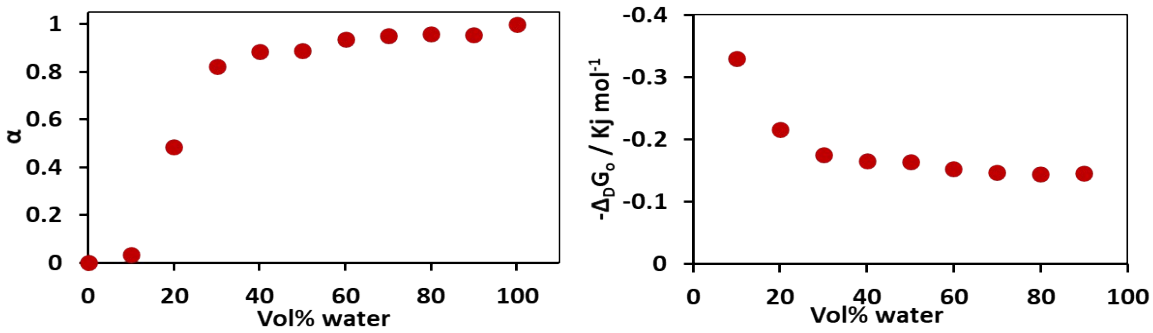

Figure S11b: Plot between degree of aggregation (α) and ΔG and volume % of water for PDI **3b**.

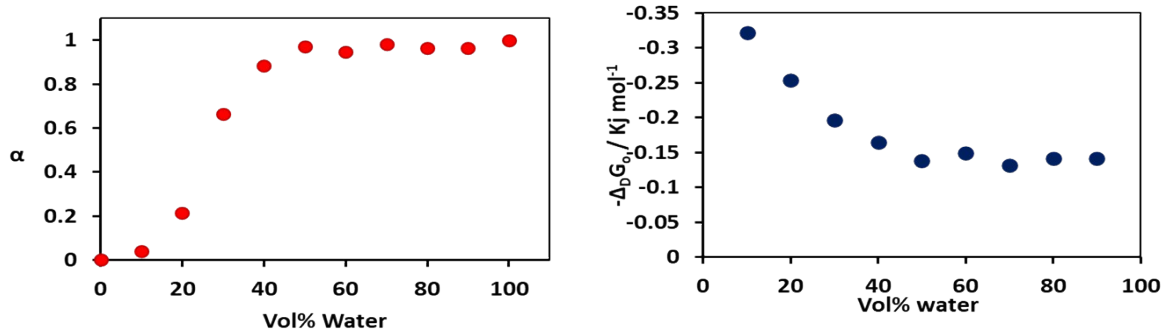

Figure S11c: Plot between degree of aggregation (α) and ΔG and volume % of water for PDI **3c**.

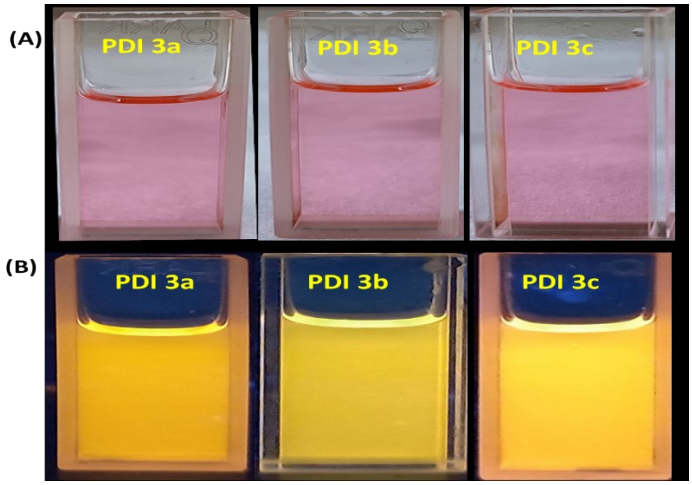

Figure S11d: Images of PDI **3**a-3c in DMSO (as monomer state) under (a) ambient light and (b) 365 nm UV lamp.

Table S1: Franck-Codon ratio of **PDI 3a-3c** derivatives.

Vol% Water	**PDI 3a**	**PDI 3b**	**PDI 3c**
0	1.438272	1.42807	1.412903
10	1.4375	1.417857	1.384365
20	1.39441	1.245283	1.361624
30	1.247839	0.88172	1.178947
40	1.102639	0.793478	0.859551
50	1.022556	0.751295	0.757576
60	1.039867	0.731844	0.722826
70	0.97992	0.732558	0.72619
80	0.895833	0.729412	0.713483
90	0.837963	0.735294	0.729885
99	0.74359	0.736842	0.753247

Table S2: Fluorescence quantum yield of PDI **3a-3c** derivatives in different water ratios.

Vol% Water	**PDI 3a**	**PDI 3b**	**PDI 3c**
DMSO	49.7	57.1	65
30	45.4	22.4	53.9
50	23.2	3.7	8.0
70	23.5	3.3	4.5
90	10.3	3.16	3.8
99	3.0	2.7	3.1

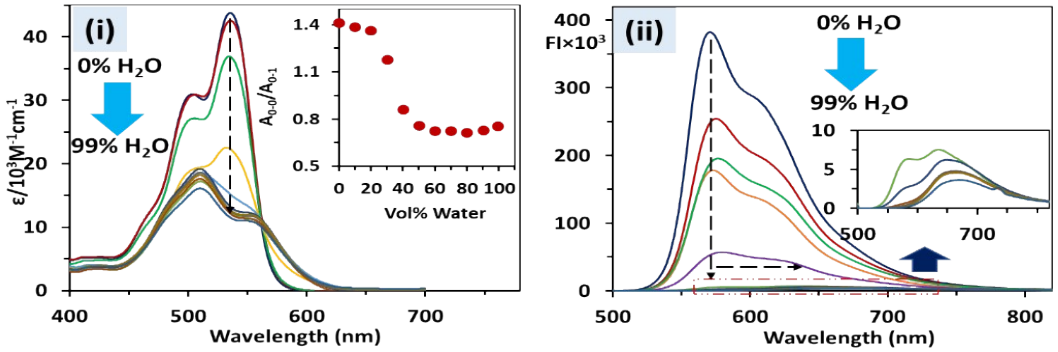

Figure S12. The UV–vis and fluorescence spectra of (i,ii) PDI **3c** derivatives showing aggregation behaviour in different H_2O: DMSO ratios. λ_{ex} = 490 nm, slit width (ex/em) =5/5.

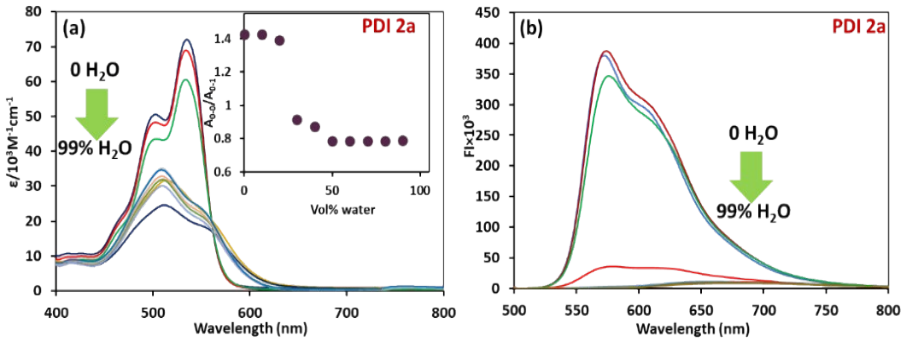

Figure S13: The UV–vis and fluorescence spectra of (a,b) PDI **2a** (10 µM) respectively showing aggregation behaviour in different DMSO-water ratios. λ_{ex} = 490 nm, slit width (ex/em) =5/5.

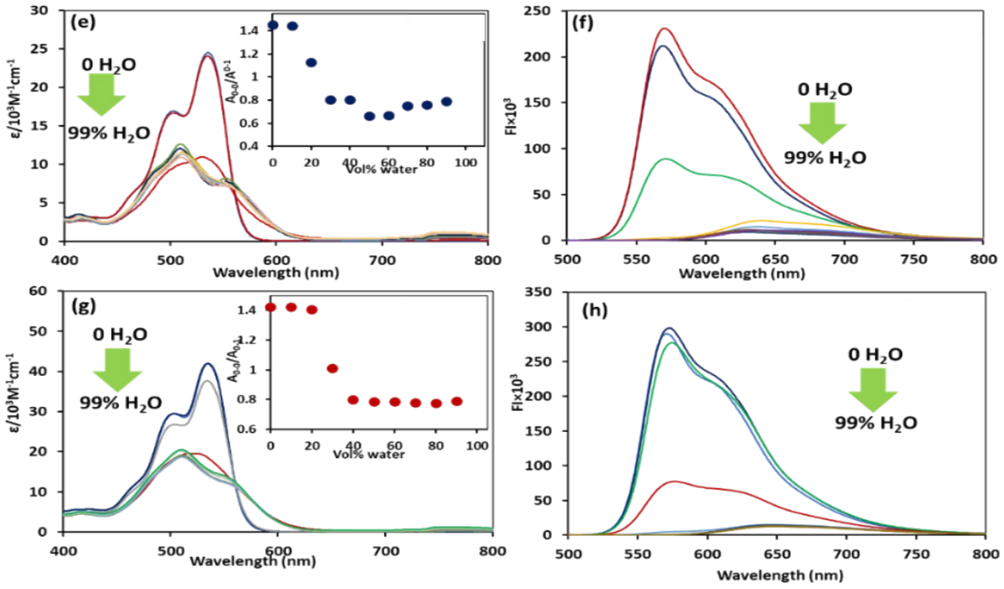

Figure S14: The UV–vis and fluorescence spectra of (e,f) PDI **2b** and (g,h) PDI **2c** (10 µM) respectively showing aggregation behaviour in different DMSO-water ratios. λ_{ex} = 490 nm, slit width (ex/em) =5/5.

Table S3: Franck-Codon ratio of **PDI 2a-2c** derivatives.

Vol% Water	**PDI 2a**	**PDI 2b**	**PDI 2c**
0	1.425743	1.449704	1.423729
10	1.423554	1.443114	1.423729
20	1.390805	1.125	1.406716
30	0.912458	0.803738	1.010989
40	0.872881	0.801887	0.798883
50	0.785714	0.661017	0.786885
60	0.783505	0.666667	0.787709
70	0.785047	0.75	0.779487
80	0.785924	0.759259	0.774359
90	0.786982	0.788991	0.790816

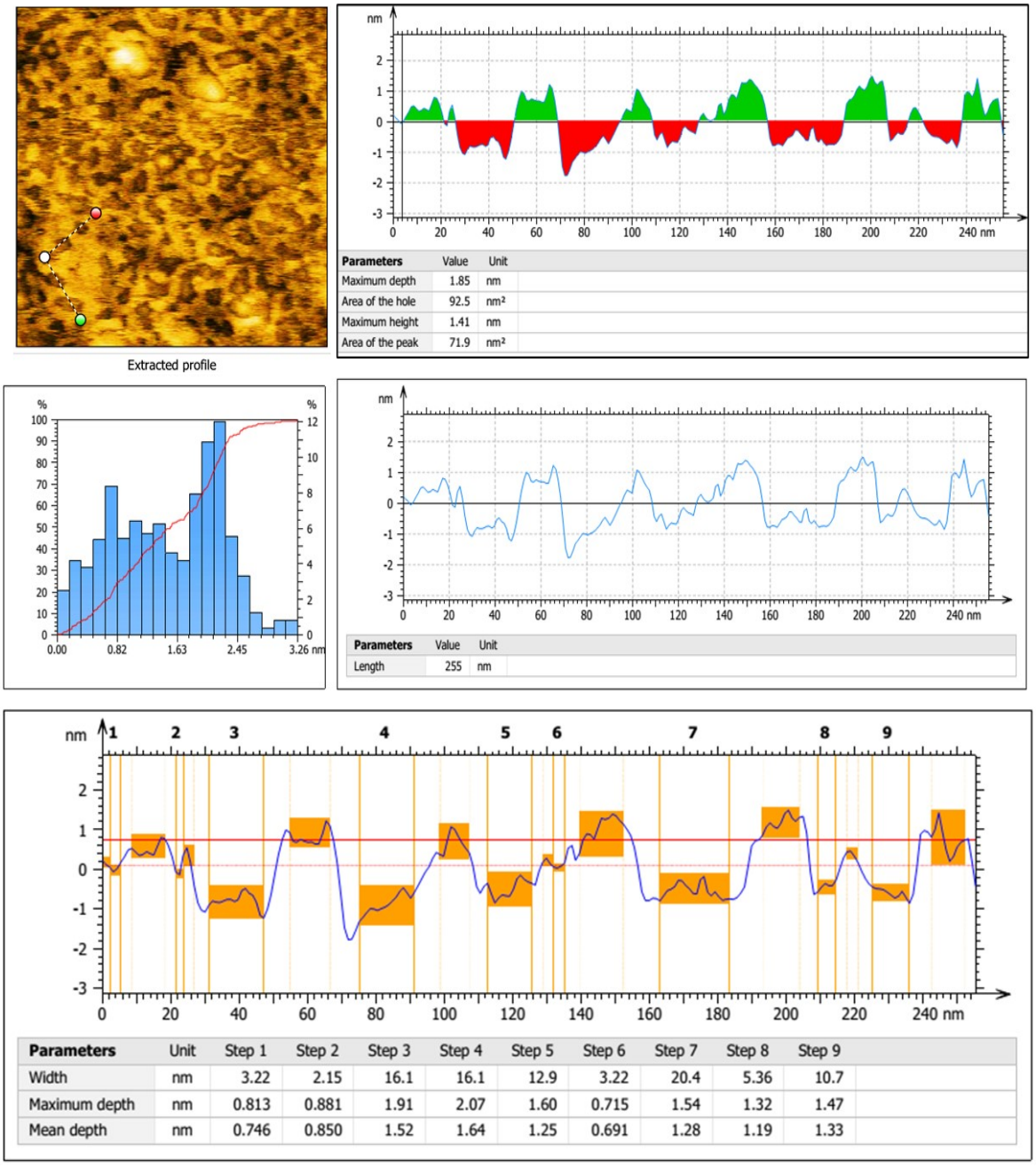

Figure S15: Extracted Height profile of PDI **3a** (1 µM).

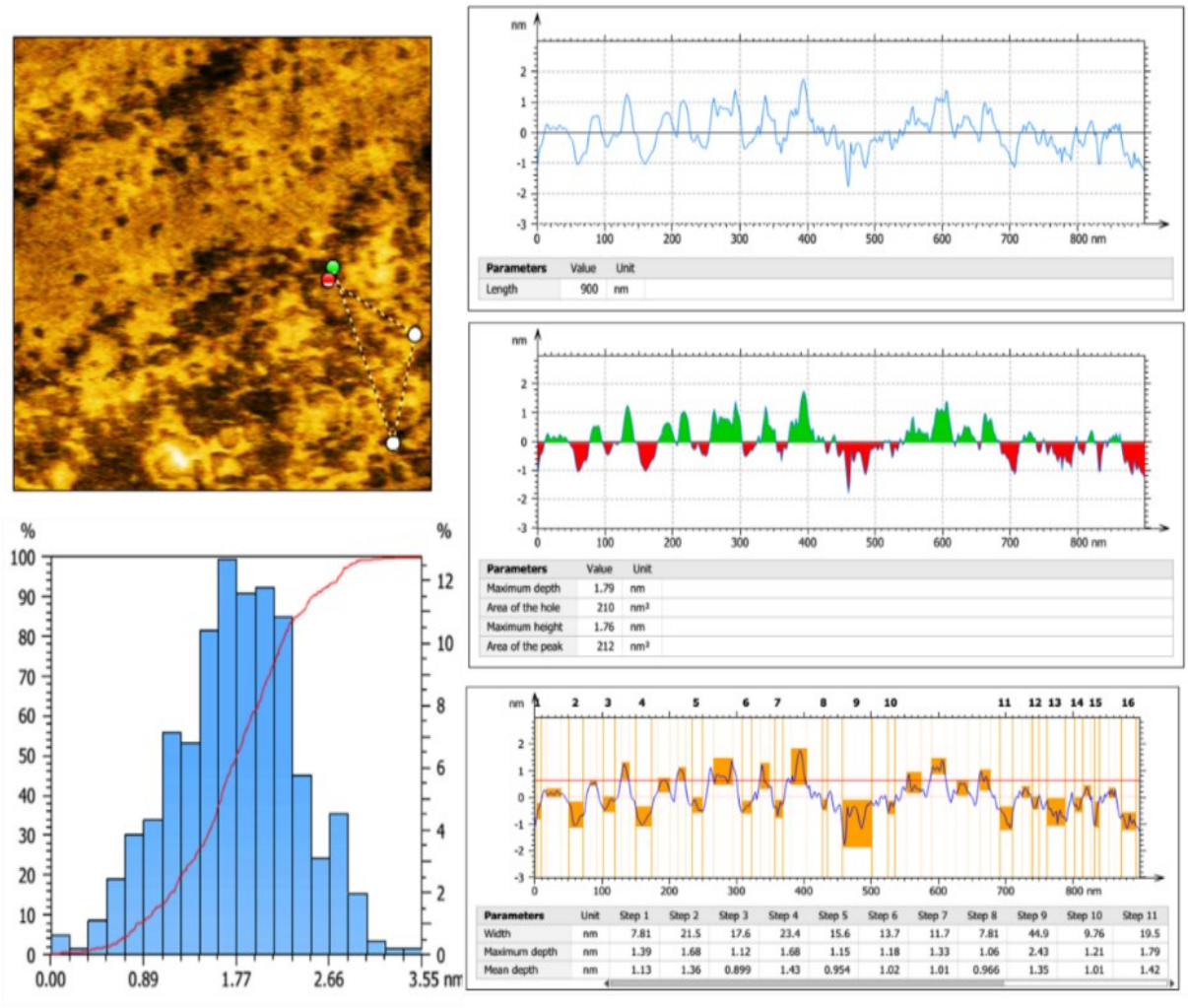

Figure S16: Extracted Height profile of PDI **3b** (1 μM).

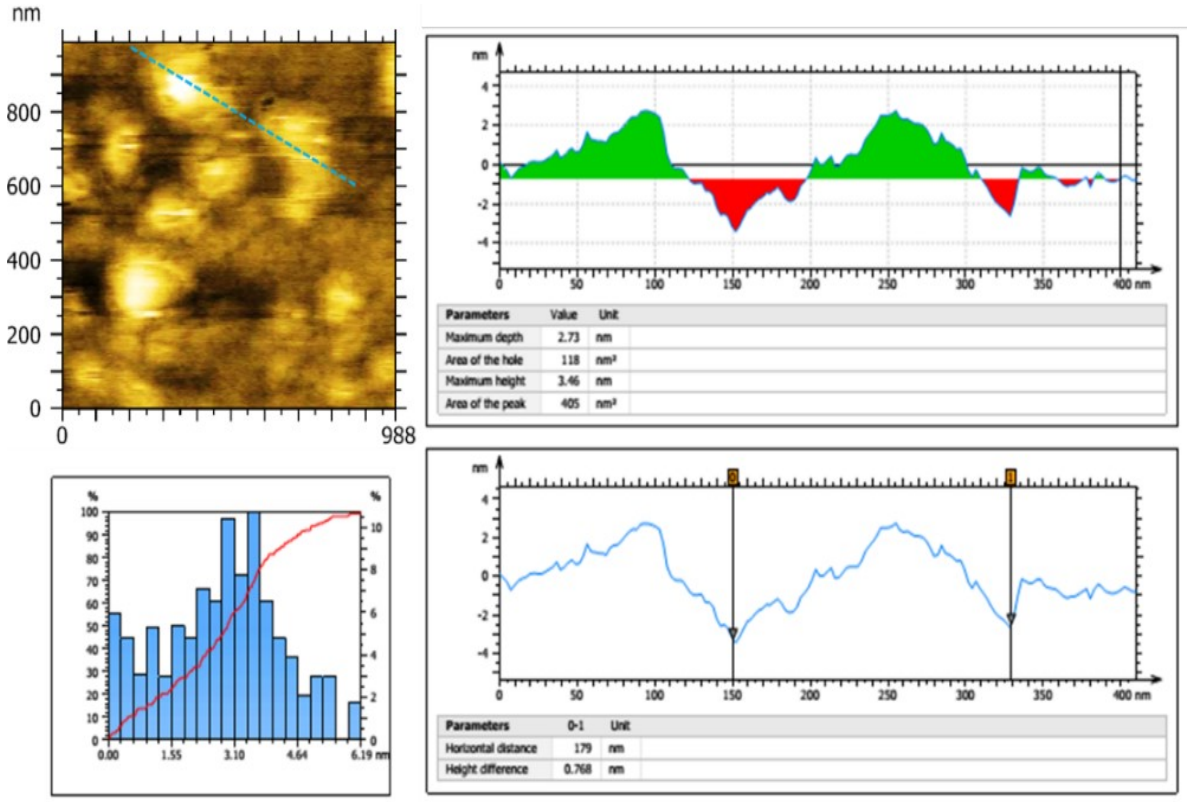

Figure S17: Extracted Height profile of PDI **3c** (1 μM).

Table S4. Spectral and photophysical characteristics of PDI **2a–2d** and PDI **3a–3d**.

Spectral Characteristics	PDI **2a**	PDI **2b**	PDI **2c**	PDI **3a**	PDI **3b**	PDI **3c**
Absorbance λ_{max} [nm]	535	535	535	535	537	536
Fluorescence λ_{max} [nm]	571	571	573	574	572	572
ε (molar absorptivity) [M^{-1} cm^{-1}]	44700	37700	69500	53500	53700	53600
Stoke Shift (in nm)	36	36	38	39	35	36
Quantum Yield (Φ in %) in DMSO	53.82	77.71	70.52	49.74	57.12	65.11
Franck-Condon Ratio (A_{0-0}/A_{0-1})	1.42	1.44	1.42	1.43	1.43	1.41
Specific optical rotation ($[\alpha]_D^{25}$)	+32.5	+15.0	+40	-90	-125	-60
HOMO Calculated from DFT (eV)	-5.832	-5.825	-5.809	-7.869	-7.878	-7.885
LUMO calculated from DFT (eV)	-3.421	-3.416	-3.418	-5.541	-5.551	-5.556
Energy gap (Eg) from DFT (eV)	2.41	2.41	2.39	2.33	2.33	2.33
HOMO calculated from CV (eV)	-5.479	-5.445	-5.559	-7.376	-7.414	-7.503
LUMO calculated from CV (eV)	-3.531	-3.602	-3.647	-5.356	-5.366	-5.31
Energy gap (Eg) from CV (eV)	1.95	1.84	1.91	2.02	2.05	2.19
λ_{ex} [nm] calculated from (TD DFT)	528.65	528.91	528.61	543.35	543.79	543.86
Angle of Twist (°)	1.48, 1.07	0.64, 1.06	1.50, 2.43	-0.79, -0.07	-0.52, 2.00	1.54, 1.55

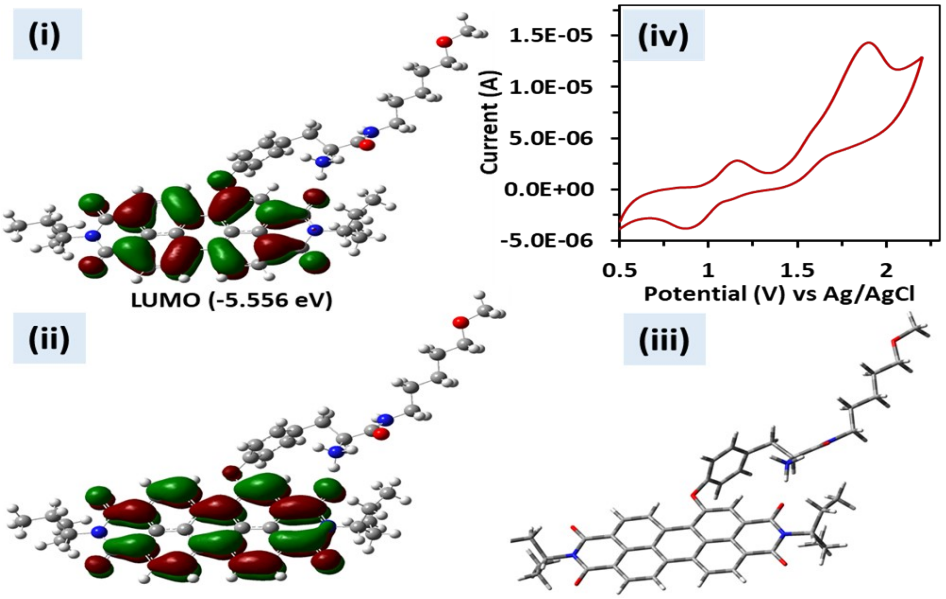

Figure S18. HOMO-LUMO molecular orbital analysis, B3LYP/6-31G* energy optimized structure and cyclic voltammograms (CV) of PDI **3c**. CV was recorded in CH_2Cl_2 solutions containing 0.1 M TBAP as supporting electrolyte with Scan rate of 50 mV s^{-1}.

3. TGA data of synthesized derivatives

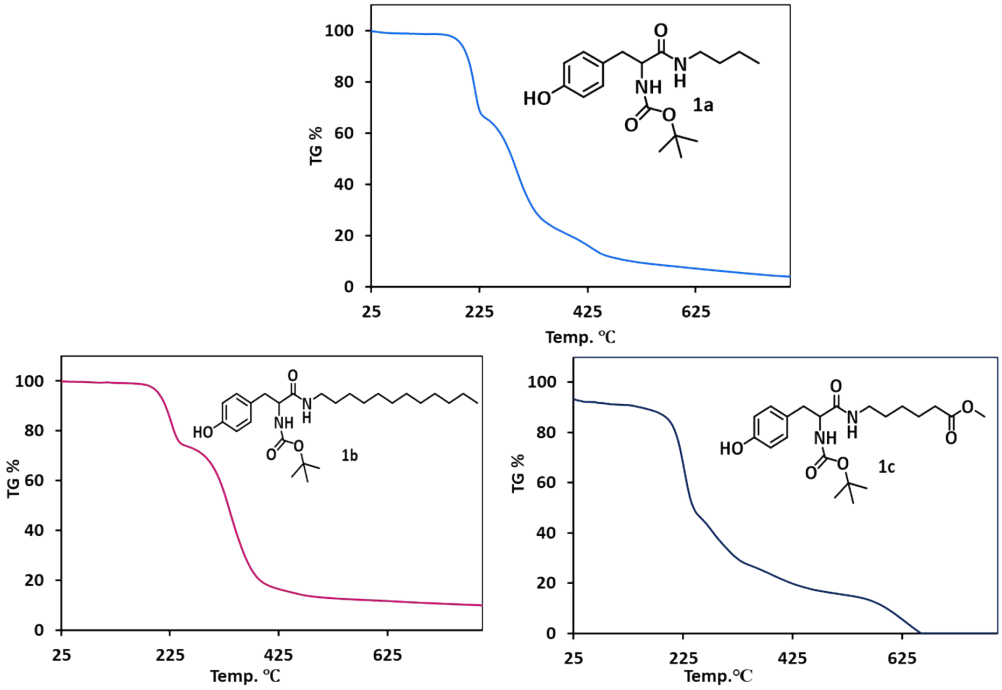

Figure S19: TGA Data of **1a-1c** derivatives.

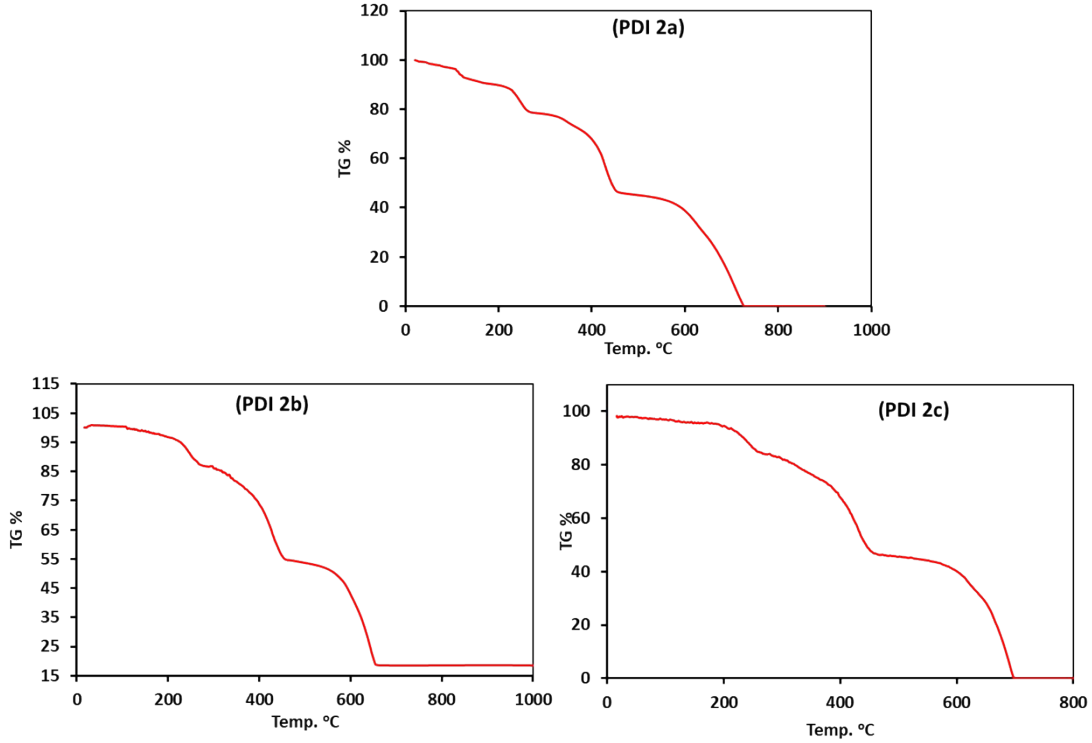

Figure S20: TGA Data of **PDI 2a-2c** derivatives.

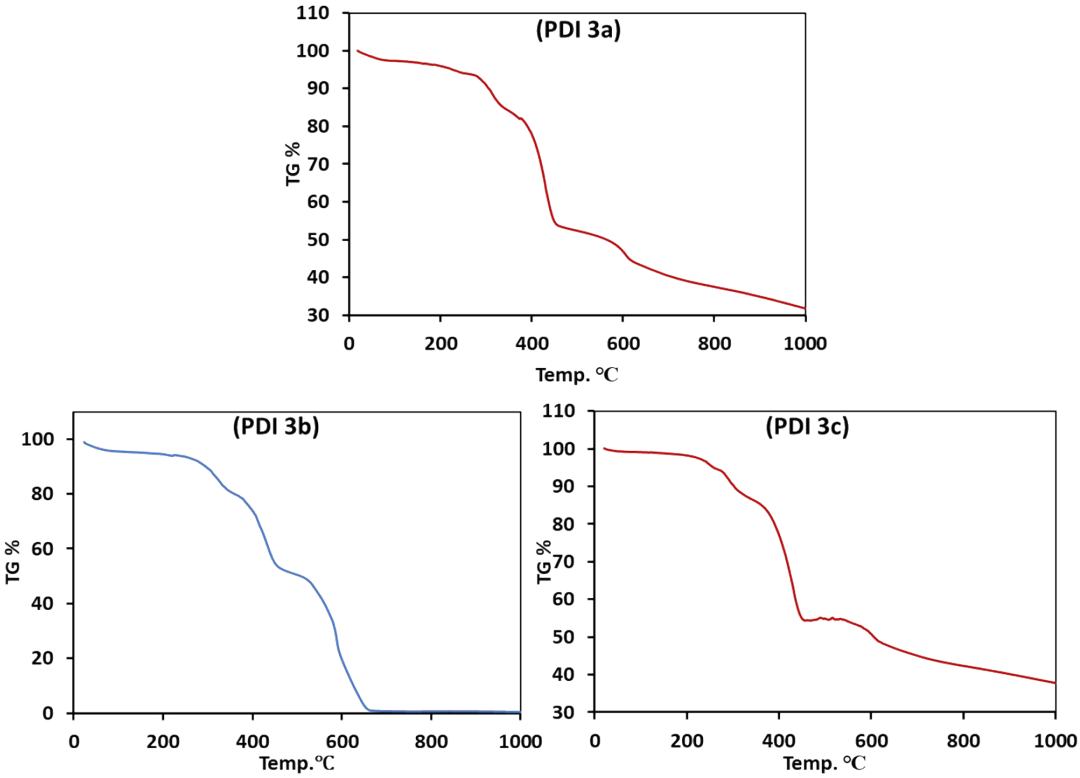

Figure S21: TGA Data of **PDI 3a-3c** derivatives.

4. Specific Optical Rotation data of 1d, PDI 2a-2c and PDI 3a-3c

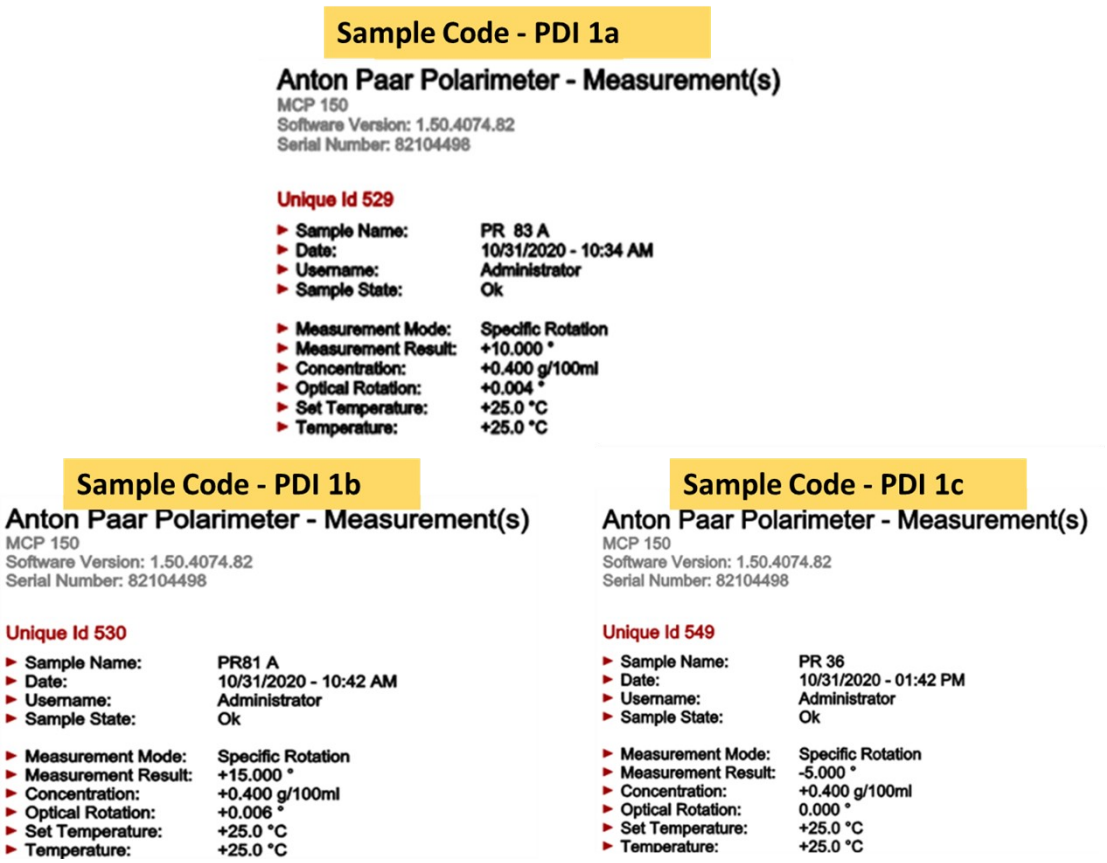

Figure S22: Specific optical rotation of **1a-1c** derivatives.

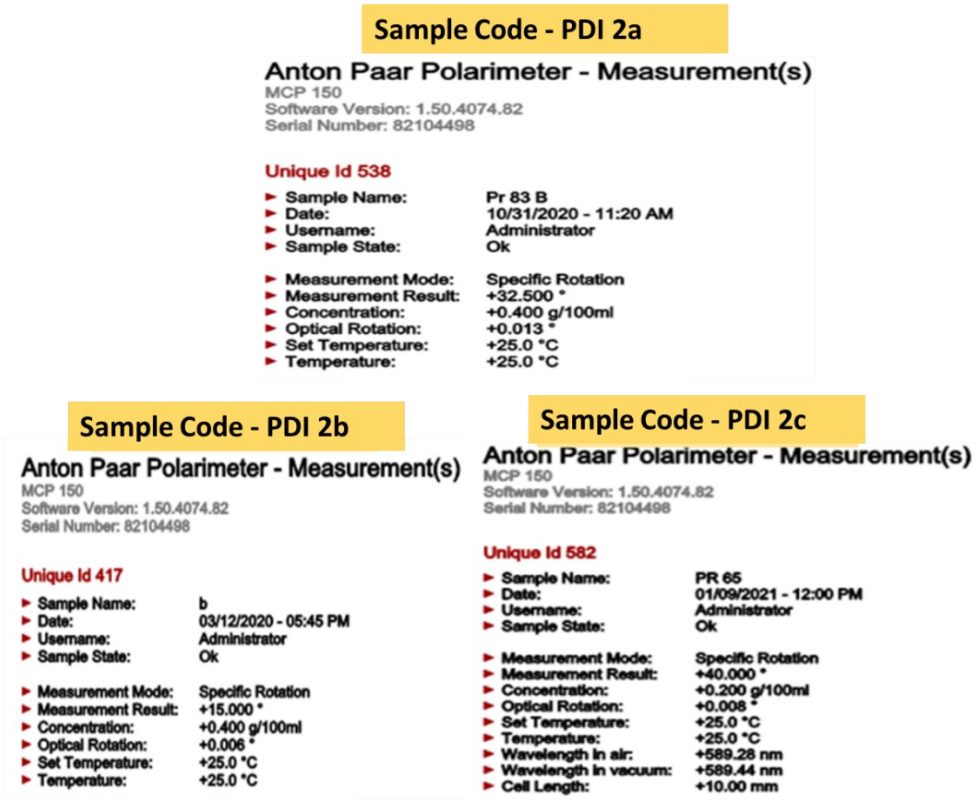

Figure S23: Specific optical rotation of **PDI 2a-2c** derivatives.

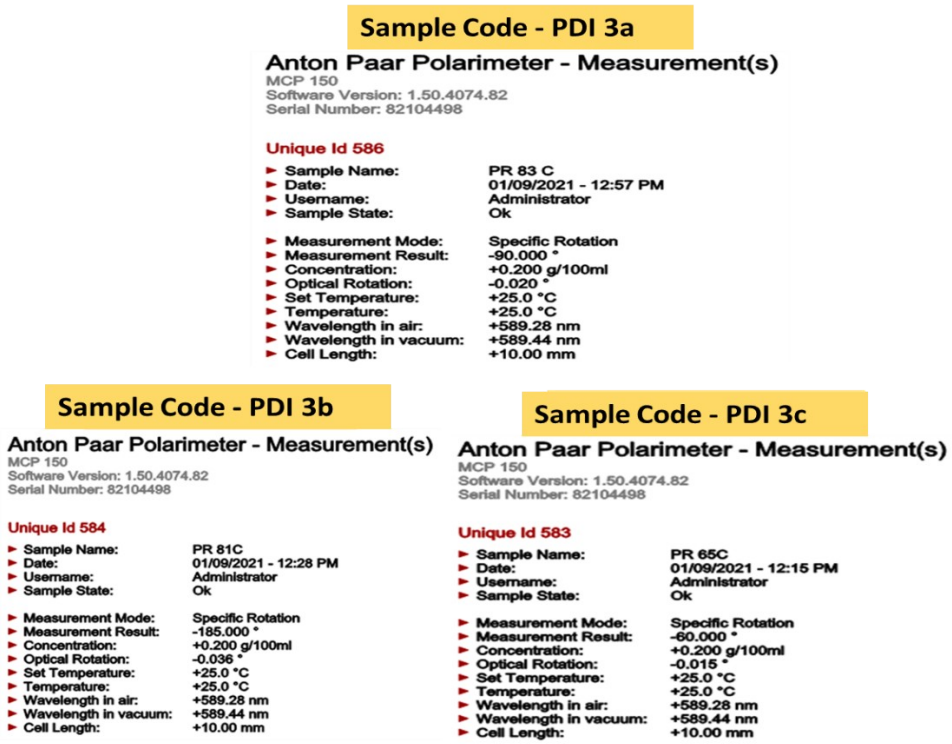

Figure S24: Specific optical rotation of **PDI 3a-3c** derivatives.

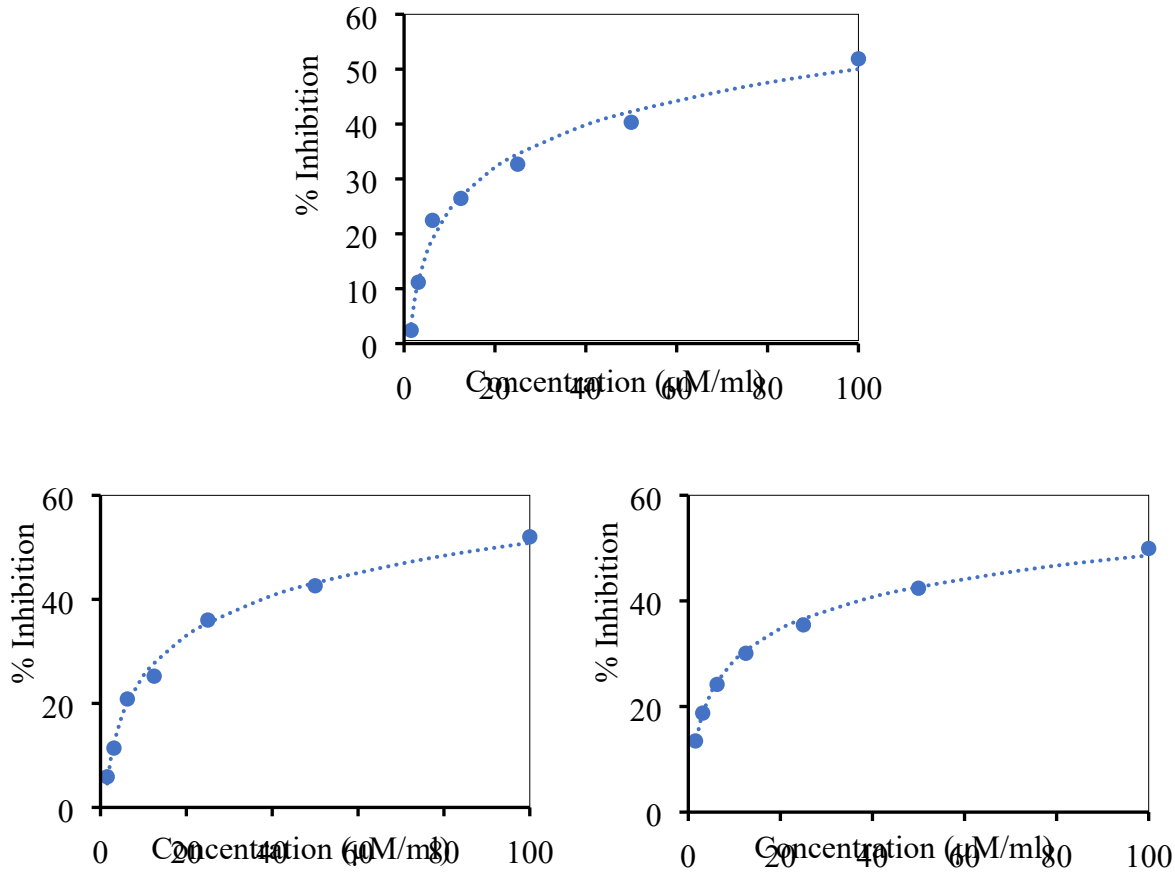

Figure S25: MTT assay of PDI **3a-c**.

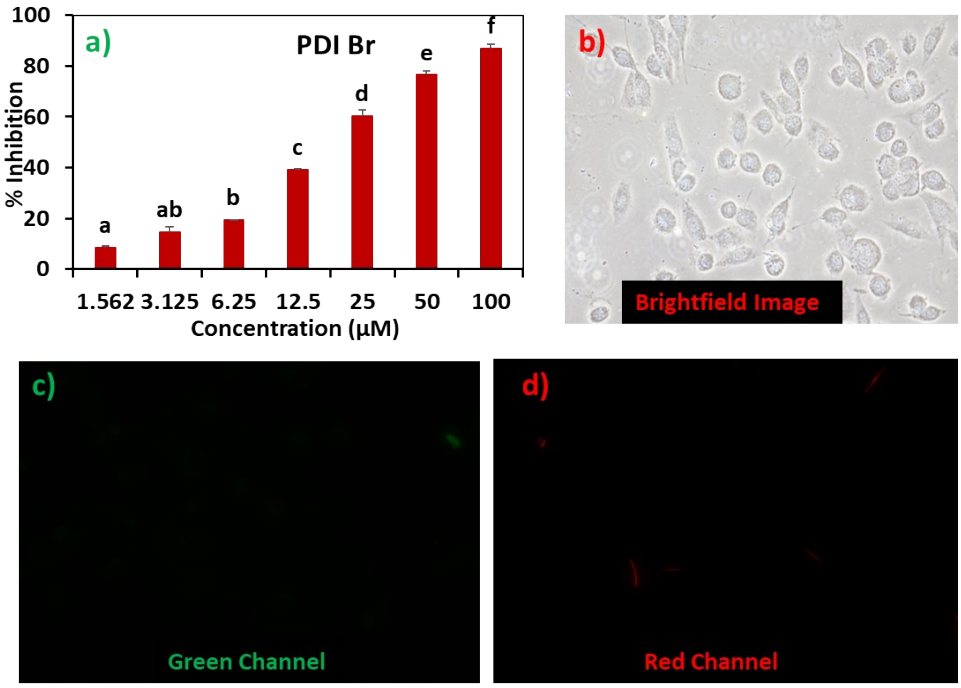

Figure S26 (a) MTT assay of PDI Br; (b) brightfield image; (c, d) fluorescence images of MG-63 cells incubated with PDI Br (1 μM) for 30 minutes.

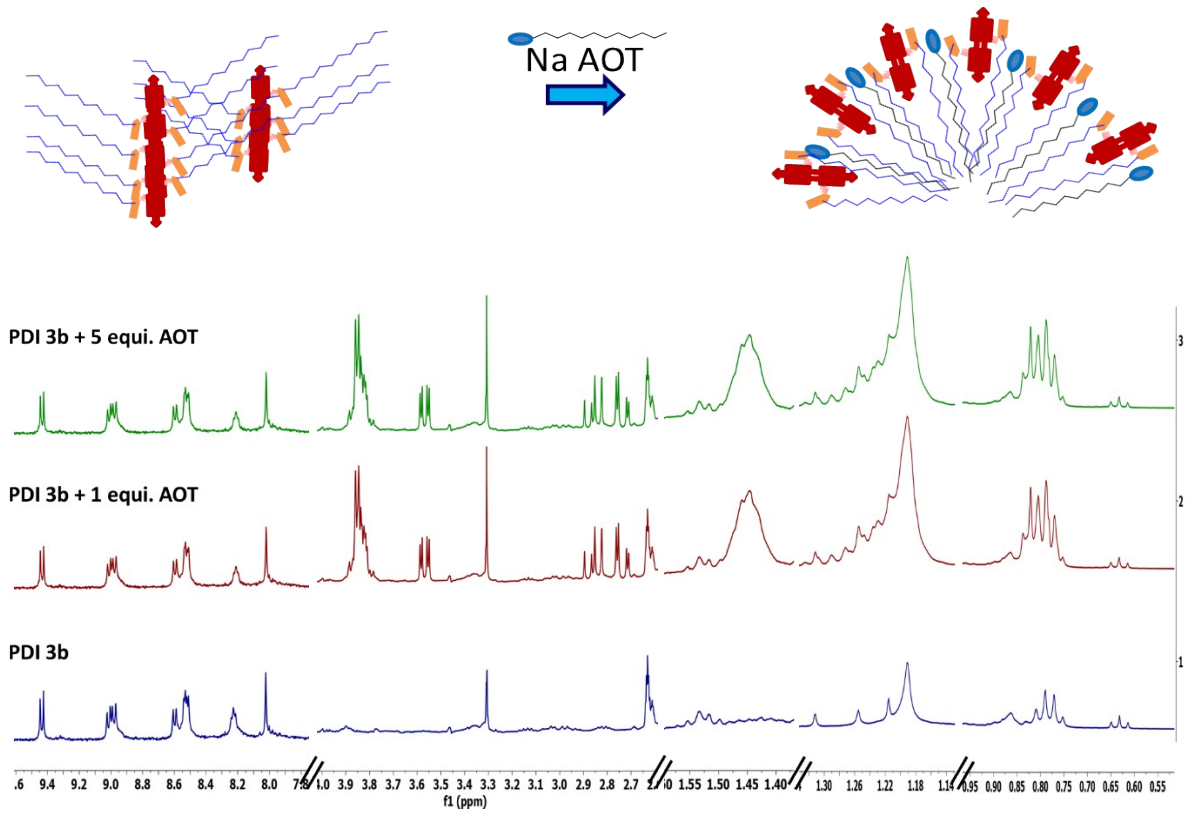

Figure S27: (top) Proposed ionic self-assembly of PDI **3b** with Na AOT and (bottom) ^{1}H NMR titration of PDI **3b** upon addition of NaAOT recorded in DMSO (d_6).